



HAL
open science

Post-translational targeting of Rab35 by the effector IcsB of Shigella determines intracellular bacterial niche formation

Nora Mellouk, Arthur Lensen, Noelia Lopez-Montero, Magdalena Gil, Camila Valenzuela, Kerstin Klinkert, Gael Moneron, Léa Swistak, David A. Digregorio, Arnaud Echard, et al.

► To cite this version:

Nora Mellouk, Arthur Lensen, Noelia Lopez-Montero, Magdalena Gil, Camila Valenzuela, et al.. Post-translational targeting of Rab35 by the effector IcsB of Shigella determines intracellular bacterial niche formation. Cell Reports, 2024, 43 (4), pp.114034. 10.1016/j.celrep.2024.114034 . pasteur-04533987

HAL Id: pasteur-04533987

<https://pasteur.hal.science/pasteur-04533987v1>

Submitted on 5 Apr 2024

HAL is a multi-disciplinary open access archive for the deposit and dissemination of scientific research documents, whether they are published or not. The documents may come from teaching and research institutions in France or abroad, or from public or private research centers.

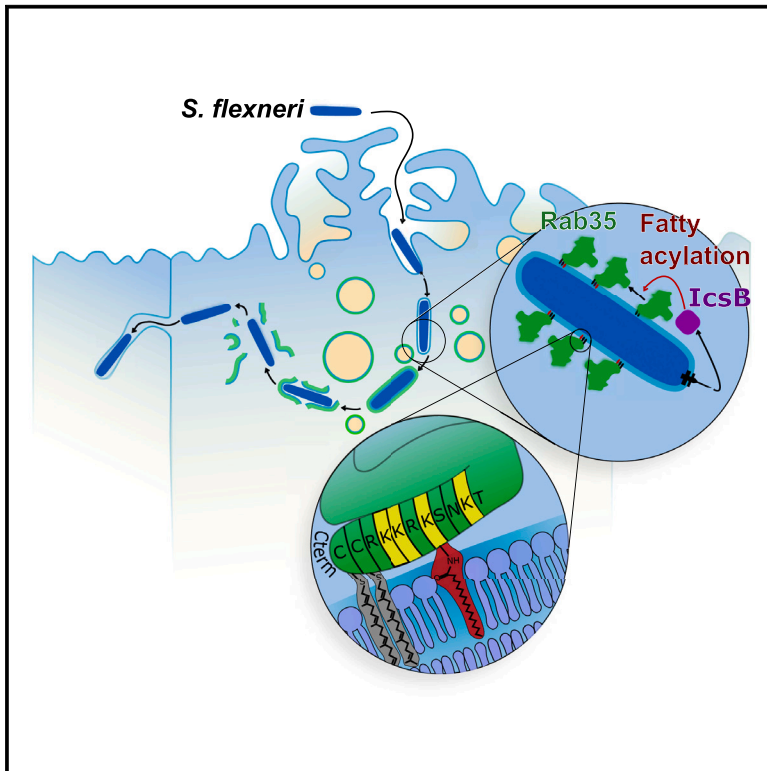
L'archive ouverte pluridisciplinaire **HAL**, est destinée au dépôt et à la diffusion de documents scientifiques de niveau recherche, publiés ou non, émanant des établissements d'enseignement et de recherche français ou étrangers, des laboratoires publics ou privés.



Distributed under a Creative Commons Attribution - NonCommercial - NoDerivatives 4.0 International License

Post-translational targeting of Rab35 by the effector IcsB of *Shigella* determines intracellular bacterial niche formation

Graphical abstract



Authors

Nora Mellouk, Arthur Lensen, Noelia Lopez-Montero, ..., David DiGregorio, Arnaud Echard, Jost Enninga

Correspondence

nora.mellouk@gmail.com (N.M.), jost.eninga@pasteur.fr (J.E.)

In brief

Shigella effectors are involved in its escape from the bacterial-containing vacuole. Mellouk et al. show that upon *Shigella* entry, IcsB post-translationally modifies Rab35 by fatty acylating lysins in its polybasic region. This entraps Rab35 at the vacuole membrane and favors release of *Shigella* into the cytosol.

Highlights

- The effector IcsB non-canonically entraps Rab35 at the *Shigella* BCV
- Lysins of the polybasic Rab35 C terminus are fatty acylated by IcsB
- Rab35 recruitment to the BCV is involved in the regulation of vacuolar disassembly



Article

Post-translational targeting of Rab35 by the effector IcsB of *Shigella* determines intracellular bacterial niche formation

Nora Mellouk,^{1,4,*} Arthur Lensen,^{1,4} Noelia Lopez-Montero,¹ Magdalena Gil,¹ Camila Valenzuela,¹ Kerstin Klinkert,² Gael Moneron,³ Léa Swistak,¹ David DiGregorio,³ Arnaud Echard,² and Jost Enninga^{1,5,*}

¹Institut Pasteur, Université Paris Cité, CNRS UMR3691, Dynamics of Host-Pathogen Interactions Unit, 75015 Paris, France

²Institut Pasteur, Université de Paris Cité, CNRS UMR3691, Membrane Traffic and Cell Division Unit, 75015 Paris, France

³Institut Pasteur, CNRS UMR3571, Synapse and Circuit Dynamics Unit, 75015 Paris, France

⁴These authors contributed equally

⁵Lead contact

*Correspondence: nora.mellouk@gmail.com (N.M.), jost.eninga@pasteur.fr (J.E.)

<https://doi.org/10.1016/j.celrep.2024.114034>

SUMMARY

Escape from the bacterial-containing vacuole (BCV) is a key step of *Shigella* host cell invasion. Rab GTPases subverted to *in situ*-formed macropinosomes in the vicinity of the BCV have been shown to promote its rupture. The involvement of the BCV itself has remained unclear. We demonstrate that Rab35 is non-canonically entrapped at the BCV. Stimulated emission depletion imaging localizes Rab35 directly on the BCV membranes before vacuolar rupture. The bacterial effector IcsB, a lysine N^ε-fatty acylase, is a key regulator of Rab35-BCV recruitment, and we show post-translational acylation of Rab35 by IcsB in its polybasic region. While Rab35 and IcsB are dispensable for the first step of BCV breakage, they are needed for the unwrapping of damaged BCV remnants from *Shigella*. This provides a framework for understanding *Shigella* invasion implicating re-localization of a Rab GTPase via its bacteria-dependent post-translational modification to support the mechanical unpeeling of the BCV.

INTRODUCTION

Shigella flexneri (referred to as *Shigella* here) is a major human intestinal pathogen that forces its uptake into non-phagocytic epithelial cells of the colon to form a bacteria-containing vacuole (BCV). For this purpose, it uses a type 3 secretion system (T3SS) to inject ~25 effector proteins into targeted host cells, which leads to the reprogramming of cellular functions.¹ A key step of the invasion process is *Shigella*-BCV rupture.^{2,3} It takes place within a few minutes upon uptake, failure to escape the BCV prevents intra- and intercellular spread of the bacterium, and it favors the targeting of the immobile BCV-entrapped pathogen by autophagy and septin pathways.^{4,5}

While entering, *Shigella* also induces the formation of infection-associated macropinosomes (IAMs) through its T3SS effector IpgD in the vicinity of the entry site.⁶ IAMs and the BCV are two distinct compartments; both need to come together to promote BCV damage.⁷ Absence of IAM formation prevents the efficient release of the bacterium into the cytosol because the pathogen remains entrapped within damaged BCVs that tightly wrap around *Shigella*.^{6,7} The identity of IAMs around the BCV has been investigated in some detail, showing host protein recruitment, including Rab guanosine triphosphatases (GTPases) Rab5 and Rab11.⁶ Purification of IAMs also identified the presence of the exocyst complex that is subverted to cluster

IAMs in proximity to the BCV.^{2,8} As it emerges that interactions between the BCV and the surrounding IAMs are key for vacuolar damage and the subsequent unwrapping of the damaged BCV membranes, it is important to understand better how host proteins are subverted at the BCV during this process.

IcsB is a key T3SS effector of the *Shigella* invasion process. It is strongly involved in the clustering of signaling proteins and actin regulators at the BCV membrane, and it has been suggested to be involved in the cytosolic access of the bacterium.^{9–13} Originally, IcsB was thought to be involved in the rupture of secondary BCVs forming in cells that become infected with *Shigella* through actin-based cell-to-cell spread from the first infected cells.¹⁴ Only later was it recognized to play a role during the early steps of *Shigella* invasion.¹³ IcsB has been linked with *Shigella* escape from autophagy in primarily invaded cells⁹ and in the formation of actin cages around the BCV, as well as septin entrapment.^{10,15} A Rho GTPase-inactivating domain has been found in IcsB, suggesting its possible interaction with host Rho GTPases, which are involved in actin cytoskeleton remodeling.^{9,10} An important study by Liu et al. discovered that IcsB triggers post-translational modifications (PTMs) on up to 60 host proteins involving Rho and Rab GTPases or SNAREs.¹¹ Detailed *in vitro* biochemical characterization has identified these PTMs as N^ε-fatty acylation by IcsB on host protein lysins.¹¹ However, the roles of IcsB N^ε-fatty acylation and substrate



specificity during the *Shigella* invasion process have remained rather unclear.

Rab GTPases are part of a large family of small GTPases that contain up to 60 members in humans.^{8,16} They ensure proper coordination of eukaryotic vesicle trafficking by regulating membrane identity, vesicle budding, fission and uncoating, motility, and fusion through the recruitment of multiple effectors.¹⁶ One of the most important features of a Rab GTPase is its localization, which is tightly linked with its function. The hypervariable C-terminal domain plays a major role in the control of Rab GTPase localization.¹⁷ This region allows lipidation at specific cysteines at the very C terminus that participate in the membrane association of the protein. Rab GTPases are frequently hijacked by intracellular pathogens, such as *Salmonella enterica*, *Listeria monocytogenes*, or *Shigella*, to induce internalization, escape of the host autophagy pathways, or better access to nutrients.^{8,16} Their subversion typically occurs through interactions with bacterial effectors acting as GTPase-activating proteins (GAPs), guanine nucleotide exchange factors (GEFs), or guanosine nucleotide dissociation inhibitors (GDIs) or by their direct subversion introducing PTMs.^{16,18} Several Rab GTPases have been found to be hijacked by *Shigella* during its invasion of epithelial cells, such as Rab11, Rab5, or Rab8.^{2,6}

Rab35 is a Rab GTPase localized at the plasma membrane and on endosomes, which controls fast endocytic cargo recycling and actin dynamics in key cellular functions, such as cytokinesis, formation of the phagocytic cup, neurite outgrowth, cell migration, and tumorigenesis.^{19–21} As for other Rab GTPases, the C-terminal polybasic region (PBR) of Rab35 is essential for plasma membrane targeting. Nevertheless, it has unique features due to the presence of a stretch of lysins upstream of the terminal cysteines that cannot be found in other Rab GTPases.²² Typically, Rab35 is recruited to endosomal membranes only for short periods in the range of minutes.²³ Activated Rab35 has been shown to interact with several host effectors, such as OCRL, Fascin, MICAL-L1, MICAL1, Podocalyxin, and ACAP2.^{23–28} It is frequently targeted by intravacuolar pathogens, for example, via ampylation or phosphocholination to re-route proteins and membranes to their vacuole, which is crucial for their survival and replication.^{29,30}

So far, Rab35 subversion has not been studied during *Shigella* invasion. We identified Rab35 as major target of the T3SS effector IcsB, leading to its immobilization at the BCV via its enzymatic acylation activity. We further demonstrated that this subversion is needed to allow unwrapping of broken BCV membranes around the entering bacteria. We suggest that our newly identified molecular cascade is crucial for *Shigella* to avoid detection by the cellular immune surveillance machinery.

RESULTS

Rab35 is recruited to *Shigella* BCV membranes in epithelial cells in a non-canonical way

We analyzed the localization of an array of Rab GTPases to the entry site of *Shigella* during challenge of epithelial cells by fluorescence microscopy (Figure S1A). Rab35 was among those to become highly enriched in the regions where the bacteria entered the host cells. To assess the dynamics of Rab35 subver-

sion during the successive steps of the *Shigella* invasion process in more detail, we performed time-lapse video-microscopy experiments of HeLa cells transfected with GFP-Rab35 or cotransfected with GFP-Rab35 and galectin-3-mOrange as marker for BCV rupture. Strikingly, GFP-Rab35 was strongly recruited to the *Shigella*-BCV prior to its rupture, in addition to some weaker recruitment to the surrounding IAMs (Figure 1A; Videos S1 and S2). Rab35 remained localized at the BCV until the end of our time-lapse series or until disassembly of the BCV membrane remnants. Importantly, this behavior was also observed in HeLa cells expressing endogenously GFP-tagged Rab35 (Figure 1B). We then tested physiologically relevant cellular models for *Shigella* invasion, namely Caco-2 TC7 and HCT-116 cells, where GFP-Rab35 was found likewise to be enriched at the BCV (Figure 1C; Video S3).

We wanted to image the localization of Rab35 around the BCV with higher precision because the BCV is surrounded with a thick actin cocoon that spans >200 nm.¹⁰ Because of this, we needed to assess whether Rab35 localized directly at the BCV membrane or more distally at the location of the actin cocoon. We addressed this with stimulated emission depletion (STED) super-resolution microscopy, a technique that allows protein localization measurements within cells below the diffraction limit in the range of tens of nanometers. With STED, we observed and characterized the localization of Rab35 down to 30 nm around the *Shigella* entering Caco-2 TC7 cells. Performing dual-color STED with the galectin-3 marker as reference for the precise localization of the membranes around entering *Shigella*, we found Rab35 localized directly at the BCV membrane (Figure 1D). The Rab35 signal partly overlapped with the galectin-3 staining (Figure 1D, left). We performed a quantitative analysis of the spatial distribution of Rab35 and galectin-3 all around the BCV through *in silico* unfolding of the BCV membranes (Figure 1D, upper right; see also STAR Methods). This clearly revealed that Rab35 never appeared more distal from the labeled BCV membranes in relation to the engulfed bacteria (Figure 1D, lower right; see also STAR Methods). Together, this analysis confirmed that Rab35 is indeed recruited directly at the BCV membrane, and it provided fine details of these structures.

The long-lasting Rab35 presence at the *Shigella*-BCV was unexpected because we anticipated its rapid replacement by Rab5 within 5–15 min, known from phagosomal maturation.^{23,31} Furthermore, we could not detect the recruitment of the Rab35 GAP EPI64B/TBC1D10B to BCVs covered with the Rab, despite its presence on the surrounding Rab35⁺ membrane ruffles and IAMs (Figure S1B). Therefore, we investigated whether Rab35 recruitment to the BCV membrane occurs in a canonical way compared to phagosomes. The internalization of *Escherichia coli* expressing an invasin A (InvA) was used as a model for canonical phagocytosis. Caco-2 cells were cotransfected with RFP-Rab35 and GFP-Rab5 and subsequently infected with either *E. coli* InvA or *Shigella* wild type (WT). The bacterial invasion of host cells was then monitored by time-lapse fluorescence microscopy for 90 min (Figures 2A and 2C; Videos S4 and S5). Analysis of the obtained time-lapse image sequences confirmed the canonical sequential recruitment of Rab35 followed by Rab5 on phagosomal membranes for *E. coli* InvA (Figure 2A). We quantified the data from our time-lapse series normalizing the

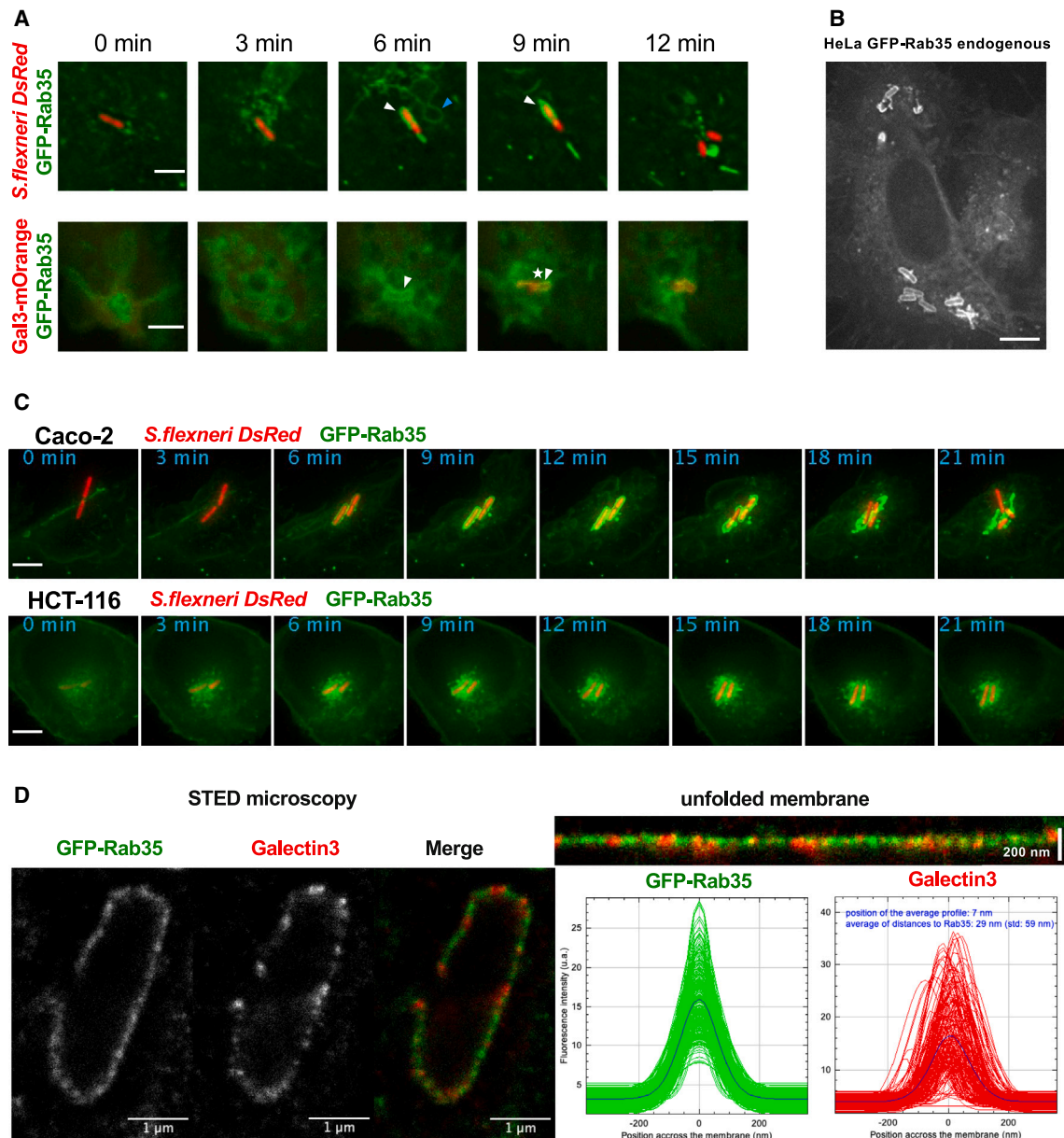


Figure 1. Rab35 is recruited to the *Shigella*-BCV in epithelial cells

Infection assays of epithelial cells transfected with GFP-Rab35, GFP-Rab35/galectin-3-mOrange and infected with *Shigella* WT or *Shigella* WT dsRed.

(A and C) Representative images of infection assay time lapses: HeLa (A) or Caco-2 TC7 and HCT-116 (C). Pictures taken from the beginning of the infection focus every 1 min, and merged (red: *S. flexneri* dsRed or galectin-3-mOrange, green: GFP-Rab35). White arrowheads: internalized bacteria. Blue arrowhead: IAM. White star: ruptured BCV. Scale bars, 5 μ m.

(B) Representative image of infection assay time lapses showing the recruitment of endogenous GFP-Rab35: HeLa GFP-Rab35^{endogenous} infected with *Shigella* WT. Scale bars, 5 μ m.

(D) Representative STED fluorescence images of fixed infection assays: Caco-2 cells transfected with GFP-Rab35 and infected with *Shigella* WT, followed by immunostaining of GFP-Rab35 (Rb anti-GFP/Gt anti-Rb StarOrange) and galectin-3 (Rt anti-galectin-3/Gt anti-Rt Atto647N). Fluorescence profiles of Rab35 across the membrane have been aligned and taken as a reference to estimate the distance between the average profiles (curves in black) of Rab35 and galectin-3, as well as for estimating the average of the distances between single pairs of profiles along the unfolded membrane.

fluorescence of the phagosomes (Figure 2B), BCVs, and IAMs (Figure 2D) in the red and green channels at each time point, taking the preinvasion background fluorescence as reference. The fluorescence intensities around the *E. coli* phagosome showed

slightly increased early Rab35 levels and strong enrichment of Rab35 from 15 min onward, with a decrease in Rab35 (Figure 2B). In contrast, *Shigella*-BCVs exhibited an early, strong, and persistent enrichment of RFP-Rab35 at their membranes, with virtually

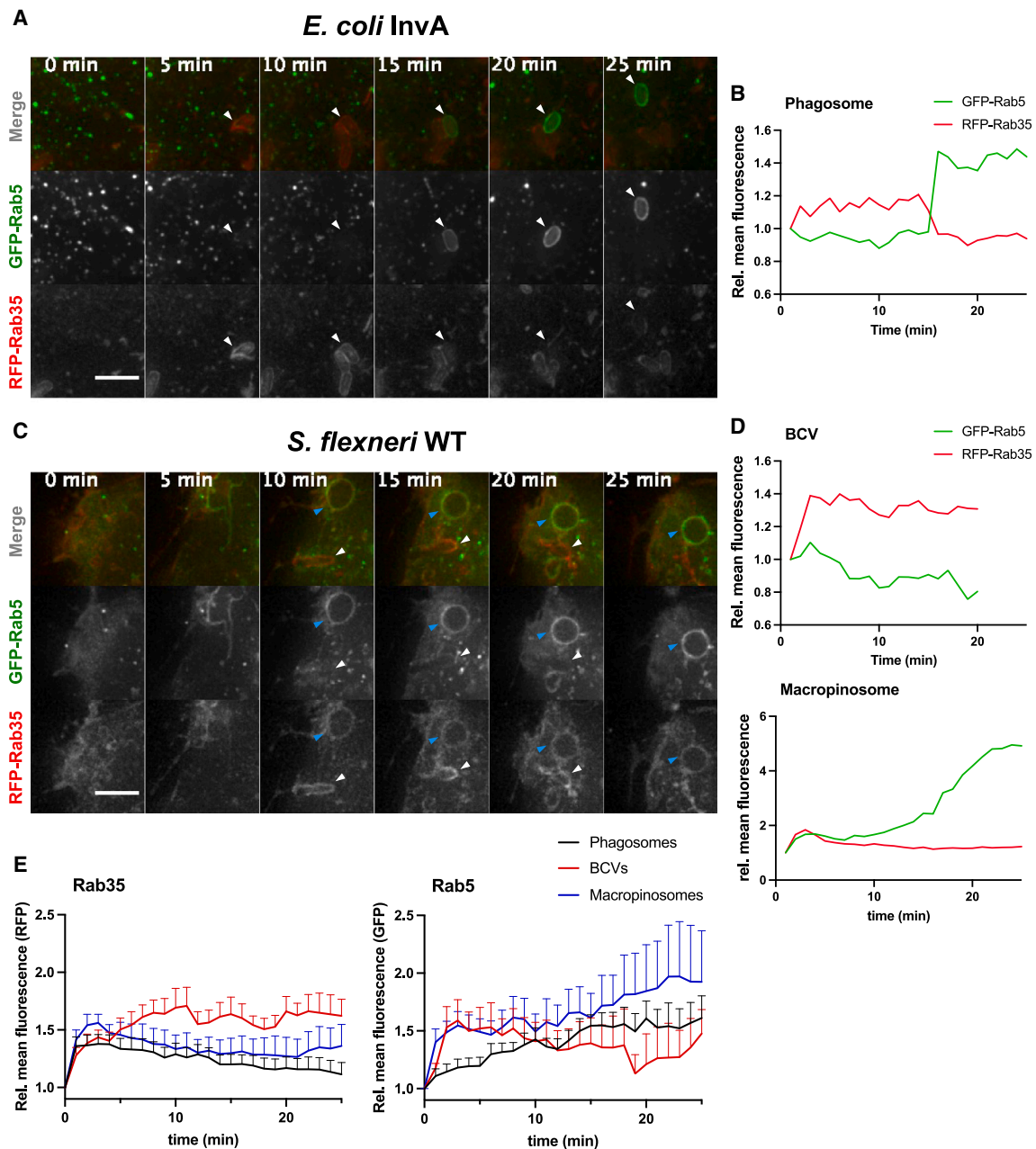


Figure 2. Canonical versus non-canonical recruitment of Rab5 and Rab35 at the BCV membrane of *E. coli* invA and *Shigella* WT

Infection assays of Caco-2 cells cotransfected with GFP-Rab5 and RFP-Rab35 and infected with *Shigella* WT or *E. coli*-expressing InvA.

(A and C) Representative images of infection assay time lapses: *E. coli* InvA (A) or *Shigella* WT (C). Pictures were taken from the beginning of the infection focus every 1 min in 2 separate channels (red: RFP-Rab35, green: GFP-Rab5) and merged. White arrowheads: internalized bacteria. Blue arrowheads: IAMs. Scale bars, 5 μ m.

(B and D) Relative fluorescence at the phagosome (during *E. coli* InvA invasion) (B) and at the BCV and IAM membrane (during *Shigella* WT invasion) (D) compared to background fluorescence intensities in the 2 separate channels.

(E) Mean fluorescence intensities of $n > 8$ plots per compartment, in both channels, analyzed from 3 independent experiments; error bars: SEM.

no GFP-Rab5 recruitment (Figure 2D). However, IAMs showed continuous enrichment in Rab5 at their membrane, whereas Rab35 levels remained very low, with a very transient Rab35 enrichment (~ 5 min post-invasion) (Figure 2D). The robustness of the distinct behavior of Rab5 and Rab35 at the BCVs, phago-

somes, and macropinosomes was confirmed by quantifying the fluorescence intensity at ~ 10 replicates for each compartment (Figure 2E). This analysis showed that RFP-Rab35 was continuously and permanently accumulated at *Shigella*-BCVs with higher intensities than on phagosomal membranes.

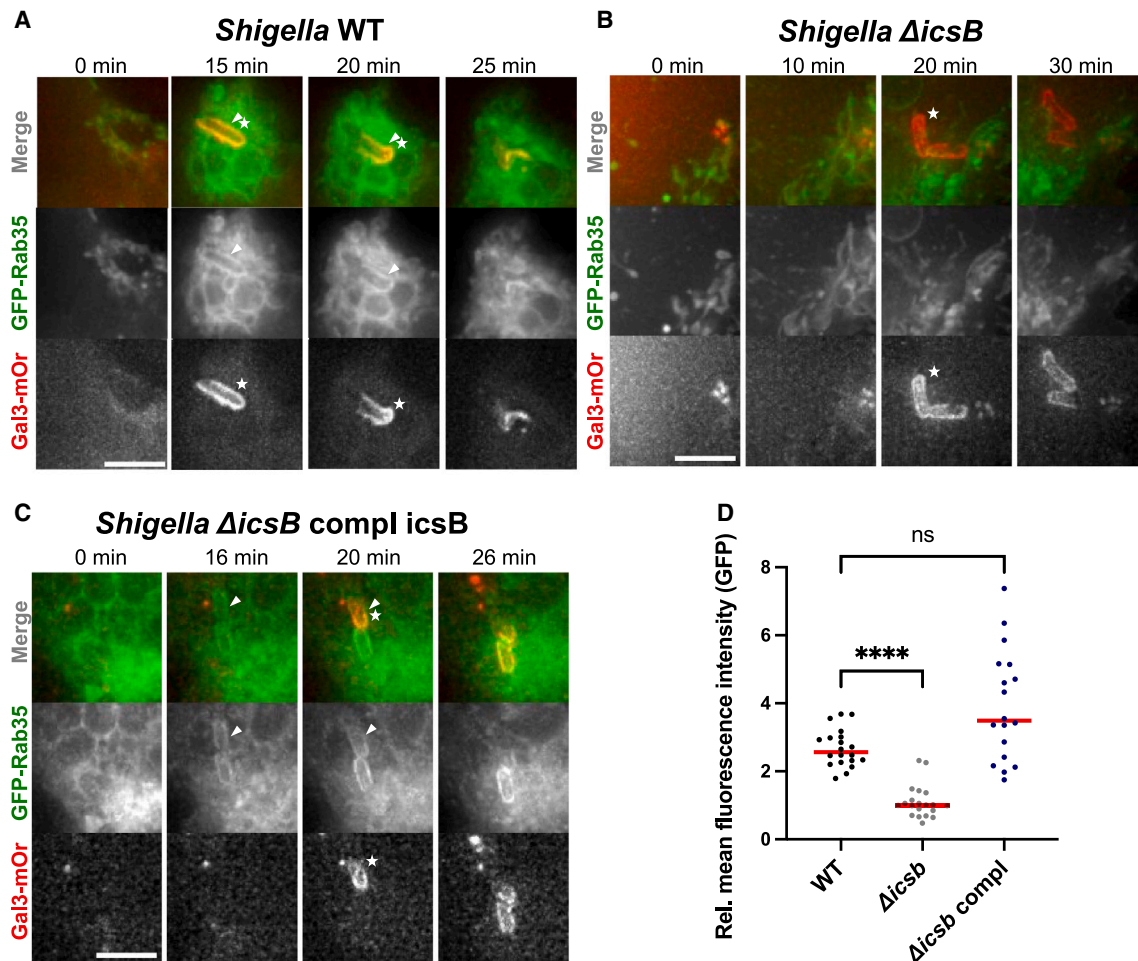


Figure 3. The bacterial N^ε-fatty acylase IcsB entraps Rab35 at the BCV

(A–C) Representative time lapses of infection assays of Caco-2 cells cotransfected with GFP-Rab35 and galectin-3-mOrange, and infected with *Shigella* WT (A), the Δ icsB (B), or the complemented Δ icsB/icsB (C). Pictures were taken from the beginning of the infection focus every 1 min in 2 separate channels (green: GFP-Rab35, red: galectin-3-mOrange) and merged. White arrowheads: internalized bacteria. White stars: ruptured BCVs. Scale bars, 5 μ m.

(D) Relative mean fluorescence intensities at the BCV just before rupture or the time point when the BCV exhibit the most intense fluorescence normalized to the average plasma membrane fluorescence intensity in the green channel (GFP-Rab35). Red bars: median (n = 20 per condition, analyzed from 3 independent experiments). Statistical significance: Kruskal-Wallis test, ****p < 0.0001, ns, not significant.

Furthermore, a few BCVs displayed a very transient and early GFP-Rab5 recruitment, which was not observed on phagosomes or IAMs. Similar results were also observed in HeLa cells, showing the impairment of the sequential recruitment of Rab35 and Rab5 at the BCV during *Shigella* invasion (Figures S2A–S2C).

Overall, these data show that Rab35 is recruited to *Shigella*-BCVs in a non-canonical way, suggesting that the internalization of this pathogen does not follow classic phagosomal maturation. This is also in line with our previous results that actively entering *Shigella* invades epithelial cells through a process that is distinct from macropinocytosis.^{7,10}

The T3SS effector IcsB targets Rab35 at the BCV

We hypothesized that Rab35 entrapment at the BCV membrane is a result of post-translational modification by a bacterial effector. IcsB has been shown recently to act as an N^ε-fatty acylase

interacting with up to 60 host proteins, among which Rab35 was identified as a potential target.¹¹ Consequently, acylation of Rab35 by IcsB could promote the tethering of this Rab GTPase to the BCV. We assessed the dynamic localization of Rab35 using a Δ icsB mutant strain for cell invasion in comparison to infections with *Shigella* WT, or the complemented Δ icsB/icsB strains. Caco-2 cells were cotransfected with GFP-Rab35 and galectin-3-mOrange and infected with the three strains. Then, we monitored the recruitment of Rab35 to the bacterial entry site by time-lapse fluorescence microscopy for 90 min, as in Figure 1 (Figures 3A–3C; Videos S6 and S7). This revealed the complete absence of any prolonged Rab35 accumulation around entering bacteria upon infection with the Δ icsB mutant. However, Rab35 was still slightly visible at the forming IAMs in proximity to the entering bacteria (Figure 3B). In addition, the complemented Δ icsB/icsB strain rescued the recruitment of GFP-Rab35 at the BCV (Figure 3C). To assess the robustness of these phenotypes,

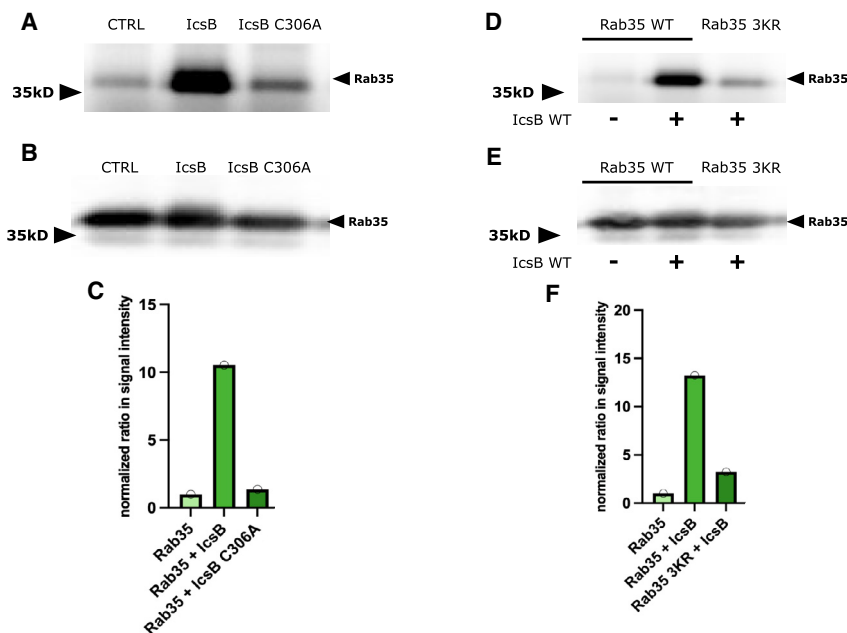


Figure 4. IcsB fatty acylates the lysines of the Rab35 PBR

Click-chemistry-based assays by in-gel fluorescence of HEK293T cells lysates previously transfected with Rab35-WT-FLAG alone (CTRL), Rab35-WT-FLAG and IcsB, or Rab35-WT-FLAG and catalytically inactive IcsB C306A (A–C) or Rab35-WT-FLAG alone, Rab35-WT-FLAG and IcsB, or Rab35-3KR-FLAG and IcsB (D–F).

(A and D) In-gel fluorescence results, bands show acylated proteins.

(B and E) Anti-FLAG western blots obtained from the gels used for in-gel fluorescence. Amounts of proteins are consistent between all conditions.

(C and F) Ratio of in-gel fluorescence signal compared to control condition (Rab35) and normalized with the corresponding western blot signal.

we proceeded with quantifications of the fluorescent signals of Rab35 around the entering bacteria. Rab35 has been shown to localize at both phagosomal compartments and the plasma membrane,²³ so the quantification of GFP fluorescence intensity was performed by normalizing the average fluorescence of the BCV at the time of its rupture to the average fluorescence of the plasma membrane at the same time point. This provided precise information on the differential Rab amounts at the BCV and the host plasma membrane, which is a proxy for the distribution of GFP-Rab35 between these two membranes (Figure 3D). For the BCVs that did not rupture during the measured time lapses, their fluorescence intensity was measured at the time point when the compartment was considered to be the most fluorescent in the green channel (GFP-Rab35). In addition, we performed time-lapse imaging of Caco-2 cells cotransfected with GFP-Rab5 and RFP-Rab35 and infected with *Shigella ΔicsB*. In contrast to the continuous and permanent accumulation of RFP-Rab35 at *Shigella* WT-BCVs (Figure 2), RFP-Rab35 did not appear around the *ΔicsB*-BCVs (Figures S2D and S2E). Our data strongly indicate an involvement of IcsB in Rab35 entrapment at the BCV.

IcsB N-fatty acylates the lysines of Rab35 PBR at the BCV

To demonstrate that Rab35 is indeed a target of IcsB, we transfected HEK293T cells with WT or mutated versions of IcsB and Rab35-WT-FLAG and performed click chemistry-based labeling of acylated proteins. Subsequently, we did immunoprecipitation and in-gel fluorescence assays following previously published protocols.^{11,32,33} Using these methods, we were able to demonstrate that Rab35-WT-FLAG is indeed fatty acylated by IcsB (Figure 4). The use of IcsB C306A (catalytically inactive) as a control further validated our results, because the acylation levels of Rab35 reverted to the same level as if no IcsB was expressed

in the cells (Figure 4A–C). IcsB-mediated fatty acylation of small GTPases, such as RhoA, relies on the targeting of one or several specific lysine residues, at least *in vitro*.¹¹ As previously noted, *in silico* analysis of the C terminus of the unconventional PBR of Rab35 highlighted the presence of a

stretch of lysines (Figures 5, lower left, and S3A).²² Because IcsB has previously been shown to fatty acylate lysines in the PBR of small GTPases, the cluster of lysines in Rab35 PBR appeared as a possible target of IcsB. To assess this, we generated a Rab35 mutant (Rab35-3KR) with the three lysines of its PBR replaced by arginines (K195R, K197R, and K198R), which is also a positively charged amino acid but cannot be enzymatically modified by IcsB. We then transfected Rab35-3KR-FLAG in HEK293T cells and repeated the same assays (Figures 4D–F). Our results showed that these lysines are preferential targets of IcsB for fatty acylation of Rab35. To consolidate our results, we incubated cell lysates with hydroxylamine (HA) to remove background cysteine acylations and obtained similar results (Figure S4).

Together, these experiments demonstrated the requirement of the N^ε-fatty acylase IcsB for the unusual recruitment of GFP-Rab35 to the BCV prior to BCV rupture as well as for the prolonged localization at the BCV membranes upon vacuolar rupture.

The Rab35 PBR is targeted by IcsB for its recruitment to the BCV

The Rab35-3KR was then investigated as to whether it was recruited to the BCV by time-lapse fluorescence microscopy of Caco-2 cells (Figures 5A and 5C; Video S8). More precisely, multiple conditions were tested similar to those presented in Figure 1, with cells being transfected either with GFP-Rab35 WT or the 3KR mutant (Figures 5A and 5B) or co-transfected with GFP-Rab35 (WT or 3KR) and galectin-3-mOrange (Figures 5C and 5D). Cells were then infected with *Shigella* WT dsRed (Figures 5A and 5B) or *Shigella* WT (Figures 5C and 5D), respectively. At first glance, the videos reveal a very faint recruitment of GFP-Rab35-3KR to the BCV membrane compared to the WT (Figures 5A and 5C; Video S8). In addition, we could still detect the accumulation of Rab35-3KR to the forming IAMs around

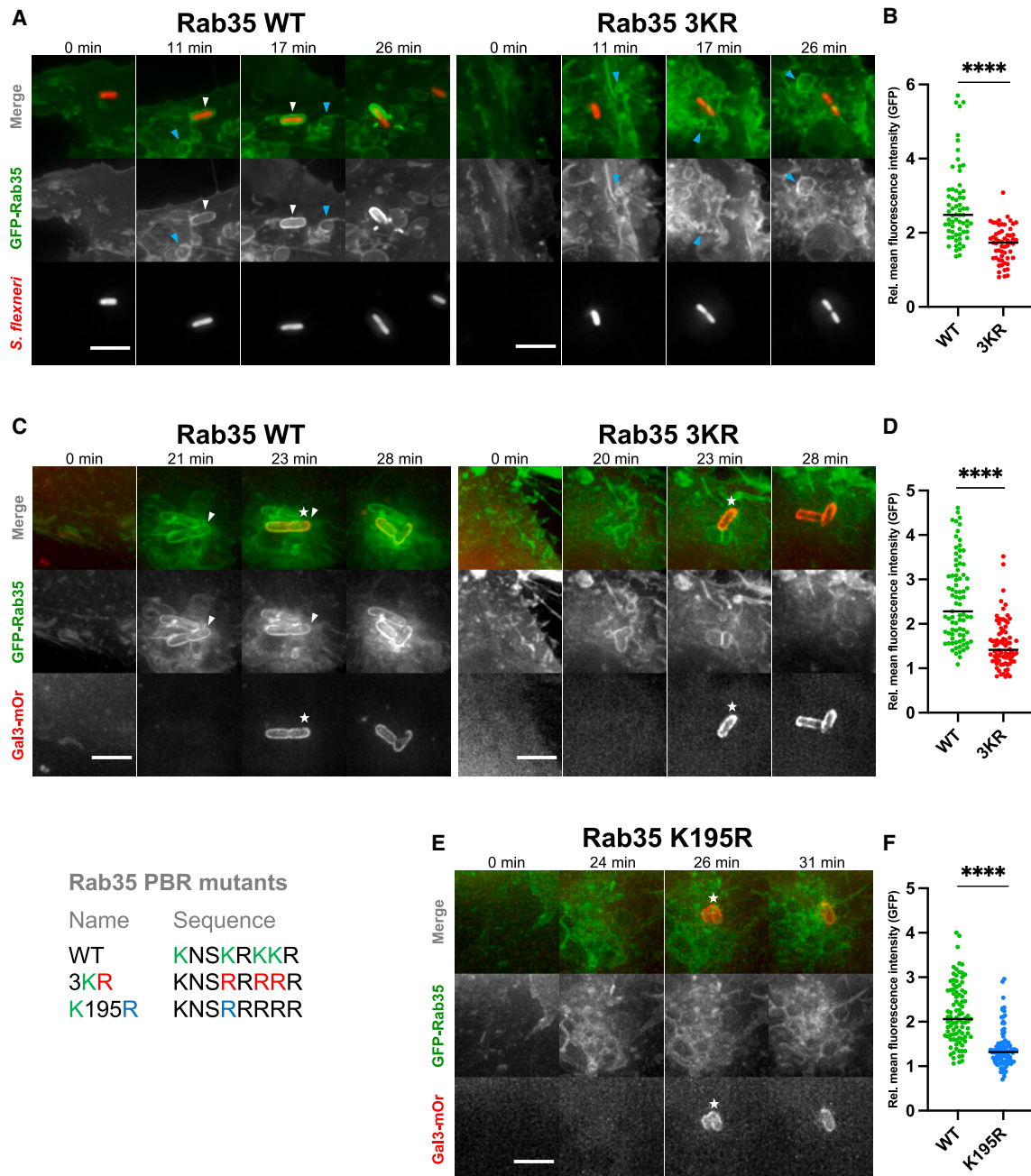


Figure 5. IcsB targets the K195 of the Rab35 PBR for BCV entrapment

The sequence of the Rab35 PBR WT, 3KR mutant (where the lysines 195, 197, and 198 were replaced by arginines), and K195R mutant (where the lysine 195 was replaced by arginine) is shown at lower left.

(A and C) Representative time lapses of infection assays of Caco-2 cells transfected with GFP-Rab35 only (WT or 3KR) (A) or cotransfected with galectin-3-mOrange (C), and infected with *Shigella* WT expressing dsRed (A) or not (C). Pictures were taken from the beginning of the infection focus every 1 min in 2 separate channels (green: GFP-Rab35, red: *S. flexneri* dsRed in A or galectin-3-mOrange in C) and merged. White arrowheads: internalized bacteria. Blue arrowheads: IAMs. White stars: ruptured BCVs. Scale bars, 5 μ m.

(B) Relative mean fluorescence intensities at the BCVs just before rupture or the time point when the BCV exhibits the most intense fluorescence normalized to the average membrane fluorescence intensity in the green channel (GFP-Rab35) in cells infected with *Shigella* expressing dsRed. Black bars: median ($n > 50$ per condition, analyzed from 3 independent experiments). Statistical significance: Mann-Whitney test, **** $p < 0.0001$.

(legend continued on next page)

the entering bacteria, similar to Rab35 WT. These results hinted at the prominent role of an intact PBR for targeting to the *Shigella*-BCV, but not to other compartments. The fluorescent signals of GFP-Rab35 WT or 3KR around the entering bacteria were quantified as in Figure 3D. These quantifications demonstrated that there is a significant difference in GFP-Rab35 recruitment upon *Shigella* invasion between the WT and the 3KR mutant, with the necessity of an intact PBR to target the *Shigella*-BCV (Figures 5B and 5D). Furthermore, Rab35 re-localization of the 3KR mutant resembled the phenotype observed with the Δ *icsB* mutant (Figure 3B).

We continued with the aim of deciphering the importance of individual lysines of the Rab35 PBR to provide further insights on the mechanism of action of IcsB. To investigate this, we made mutants in which one or several lysines were replaced by arginines (Rab35-2KR and Rab35-K195R, where the lysines 197 and 198 or the lysine 195 were replaced by arginines, respectively). Then, time lapses were performed in Caco-2 cells cotransfected with GFP-Rab35 (WT, and the mutated proteins) and galectin-3-mOrange after infection with *Shigella* WT. This identified that the GFP-Rab35-K195R mutant shows strong inhibition of its recruitment at the BCV compared to the WT (Figures 5E and 5F; Video S9). In contrast, the GFP-Rab35-2KR mutant showed recruitment similar to that of WT (Figures S3B and S3C). To distinguish between the wrapping and the unwrapping of ruptured BCVs, we performed time-lapse confocal imaging of Caco-2 cells cotransfected with GFP-Rab35 and galectin-3-mOrange and infected with *Shigella* WT BFP (Figure S5).

Our combined data suggest that the lysine 195 of GFP-Rab35 is crucial for IcsB-mediated subversion of Rab35 at the *Shigella*-BCV, and a synergistic effect of additional PBR lysines may occur.

Rab35 recruitment to the BCV promotes *Shigella* vacuolar membrane unpeeling within primary infected cells

We then asked, what is the role of Rab35 subversion at the BCV for the course of *Shigella* infection? Because Rab35 is recruited before vacuolar rupture, we hypothesized that it could be involved during the early events of *Shigella* intracellular niche formation. Vacuolar rupture involves a sequence of steps. It starts with initial membrane destabilization and BCV damage, eventually leading to the complete unwrapping of the enclosed bacteria to allow their efficient intra- and intercellular spread. Taking full advantage of the galectin-3-GFP reporter, we are able to pinpoint both the initial step of membrane damage and the fate of the damaged membranes. To monitor this, we first generated HeLa CRISPR Rab35 knockout (KO) cells and characterized them. The level of Rab35 expression in HeLa CRISPR Rab35 WT or KO cells was measured by western blot, showing the absence of the protein in the KO cells (Figure S6A). Upon transfection of the Rab35 KO cells with galectin-3-GFP, we infected them with *Shigella* WT dsRed. Inspecting

the time-lapse videos, we noticed a striking difference for both conditions, with *Shigella* remaining entrapped within damaged BCVs, in the case of the Rab35 KO, whereas the BCV membranes unwrapped rapidly in WT conditions, with membrane pieces moving away several micrometers within a few minutes (Figure 6A; Video S10). Quantifying these events corroborated that bacterial entry foci formation was slightly delayed in the Rab35 KO cells (Figure S6B), whereas the onset of vacuolar rupture upon foci formation (Figure 6C) was unchanged. However, the time span of BCV disassembly was dramatically delayed in the Rab35 KO cells, indicating that the efficient unwrapping of the damaged BCV membranes (Figure 6D) could not take place, leading to delayed intracellular bacterial motility (Figure 6E). The expression of GFP-Rab35 WT or Rab35-FLAG but not GFP-Rab35-3KR mutant restored the efficient unwrapping of the ruptured BCV in Rab35 KO cells (Figures 6A, S7A, and S7B), suggesting that the IcsB targeting of Rab35 to the BCV membrane plays a role in the cytosolic escape of *Shigella* within primary infected cells. We performed indirect immunofluorescence labeling of Rab35-FLAG to control that all galectin-3-GFP-expressing cells also expressed Rab35 (Figure S7C). In HeLa cells expressing Rab35, *Shigella* Δ *icsB* remained entrapped within BCVs compared to invasions with *Shigella* WT (Figure 6B), resembling *Shigella* WT invasions in Rab35 KO cells (Figure 6A). This phenotype is in agreement with what has been previously described by Kühn et al.¹⁰

After the rupture of the initial vacuole, *Shigella* replicates rapidly within the host cytosol and it spreads from cell to cell. To achieve this, it propels itself from a first infected cell into neighboring cells, forming actin comet tails. In the neighboring infected cells, *Shigella* then escapes so-called secondary vacuoles. This step does not involve the formation of IAMs that need to interact with the BCV crucial for BCV damage and unwrapping in the first infected cell.^{2,7} To measure whether these later steps of infection were affected through the IcsB-Rab35 axis, we measured the formation of infection focus in fully confluent Caco-2 cells upon infection with *S. flexneri* WT or Δ *icsB* at a very low MOI of 0.05. Under these settings, an infection focus is formed upon cell invasion with only one bacterium. The area of each cell infection focus was measured, and we observed that compared to the WT strain, the Δ *icsB* mutant presents smaller plaques, indicating a restricted cell-to-cell spread (Figures 6F and 6G).

Altogether, our results suggest that the reprogramming of Rab35 at the BCV via the IcsB-induced acylation contributes to the efficient unwrapping of *Shigella* from the damaged vacuole. Moreover, the absence of IcsB decreases the efficiency of cell-to-cell spread.

DISCUSSION

The paradigm how *Shigella* forms its intracellular niche in epithelial cells has changed over the last several years.³ It has become

(D) Relative mean fluorescence intensities at the BCVs just before rupture or the time point when the BCV exhibits the most intense fluorescence normalized to the average membrane fluorescence intensity in the green channel (GFP-Rab35) in cells co-transfected with galectin-3-mOrange and GFP-Rab35. Black bars: median ($n > 50$ per condition, analyzed from 3 independent experiments). Statistical significance: Mann-Whitney test, **** $p < 0.0001$.

(E) Representative time lapses of infection assays of Caco-2 cells cotransfected with GFP-Rab35-K195R and galectin-3-mOrange, and infected with *Shigella* WT. Pictures were taken from the beginning of the infection focus every 1 min in 2 separate channels (green: GFP-Rab35, red: galectin-3-mOrange) and merged. White star: ruptured BCV. Scale bars, 5 μ m.

(F) Relative mean fluorescence intensities at the BCVs just before rupture or the time point when the BCV is the most fluorescent, normalized to the average membrane fluorescence intensity in the green channel (GFP-Rab35). Black bars: median ($n > 90$ per condition, analyzed from 3 independent experiments). Statistical significance: Mann-Whitney test, **** $p < 0.0001$.

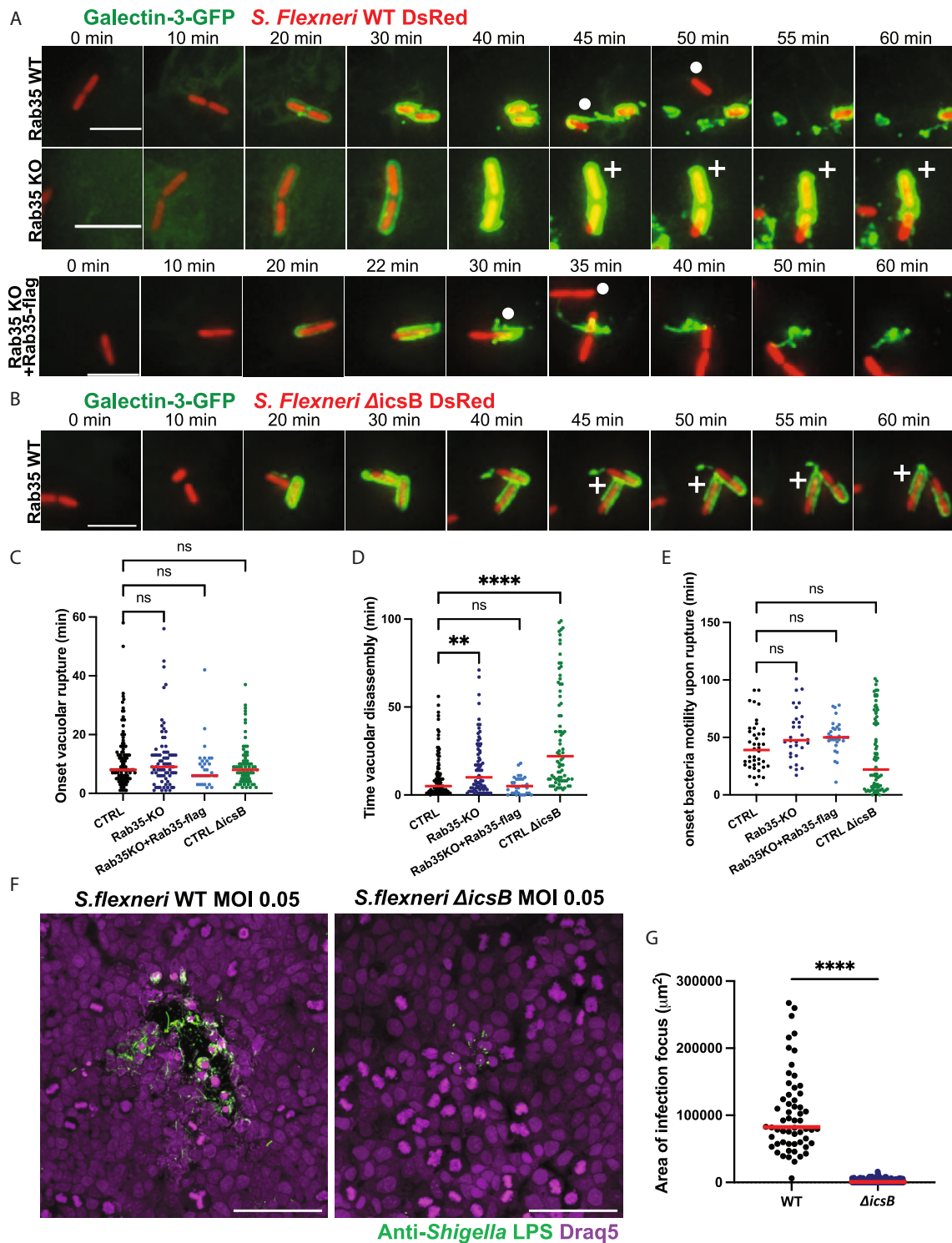


Figure 6. Rab35 entrapment at the BCV is required for *Shigella* vacuolar membrane unpeeling and cell-to-cell spread

(A and B) Representative time lapses of infection assays of HeLa CRISPR Rab35 WT or Rab35 KO cells transfected with galectin-3-GFP only or cotransfected with Rab35-WT-FLAG and infected with *Shigella* WT dsRed (A) or *Shigella* Δ icsB dsRed (B). Pictures were taken from the beginning of the infection focus every 1 min in 2 separate channels (green: galectin-3-GFP, red: *S. flexneri* dsRed) and merged. White circle: time of *Shigella* vacuolar membrane unpeeling. White cross: *Shigella* remaining entrapped within damaged BCV. Scale bars, 5 μ m.

(legend continued on next page)

clear that the pathogen does not enter actively through macropinosytosis; however, two events take place simultaneously—bacterial entry within a thus far poorly characterized phagosome or BCV and the formation of IAMs that make contact with the phagosome to promote vacuolar rupture.^{2,6,7} IAM reprogramming and recruitment to the BCV before its damage have already been characterized in some detail.^{2,7} Here, we show the massive subversion of Rab35 to the *Shigella*-BCV, making Rab35 a robust marker for this compartment (Figure 1). The strong and permanent recruitment of Rab35 to the BCV membrane while Rab5 is virtually absent pointed toward a non-canonical targeting pathway (Figure 2). Mechanistically, the addition of fatty acylation on the lysines of the Rab35 PBR by the bacterial effector IcsB could explain this massive and atypical entrapment of Rab35 at the BCV (Figures 3, 4, and 5). In case Rab35 is absent, the onset of BCV rupture is not altered; however, the broken membrane remnants cannot be peeled away from the entering bacteria (Figure 6). This phenotype is the same when IAM formation is abrogated (by depleting the T3SS effector IpgD), or similar to infections with the Δ icsB mutant (Figure 6).^{6,10} It underscores a functional link between the BCV and the surrounding IAMs for the unwrapping of the entering bacteria. Therefore, it is tempting to speculate that Rab35 acts as an anchor making membrane contacts with the forming IAMs. Rab35 effectors or interactors, such as the MICAL-L1 proteins, could play a role in the formation of stable complexes between both compartments, which should be tested in future studies. Furthermore, it needs to be investigated how such complexes can convey the mechanical forces driving the broken BCV membranes away several micrometers from the entering bacteria. It is likely that motor proteins present on the IAMs play a role in this process.²

Rab35 is modified differently by several other pathogens to promote bacterial intracellular survival or replication. For instance, *Legionella pneumophila* induces Rab35 AMPylation and phosphocholination, ultimately leading to its depletion by reducing Rab35 binding to its GEF DENND1A.³⁴ The subversion of Rab35 by *Legionella* effectors redirects the exocytosis pathway to control the transport and the formation of the membrane-bound compartment in which the bacterium resides. On the other hand, uropathogenic *E. coli* (UPEC) enhances the expression of Rab35 to escape lysosomal degradation and enhances iron uptake into the BCV. Indeed, Rab35 is involved in transferrin receptor recycling, which is responsible for transferrin-mediated cellular iron uptake, and its subversion by UPEC promotes its survival.³⁵ Here, our work identifies a key role of Rab35 acylation for the unwrapping of the BCV membrane remnants during *Shigella* invasion. This step appears crucial to render the bacteria naked within the cytosol for actin-based motility. Together, it highlights the role of Rab35 as a major trafficking regulator being relevant for different infection processes.

PTM modification of host factors is a common theme during the intracellular niche formation of *Shigella*.³⁶ Exemplarily, this can either perturb the stability of host proteins through ubiquitination via the IpaH family³⁷ or affect the innate immune signaling events through OspF or OspC3.^{38,39} Furthermore, *Shigella* effectors also act as proteases (IpaJ), glutamine deamidases (OspI), or methylases (OspZ) to modify host responses.^{40–43} Recently, Liu et al. found that numerous host proteins become N^ε-fatty acylated by IcsB on lysines.¹¹ IcsB was found to interact with up to 60 host proteins, including Rab35, and it was shown that its 18-carbon acyltransferase activity catalyzes fatty acylation on the C terminus of RhoA *in vitro*.¹¹ It remains to be elucidated how substrate specificity of IcsB is achieved. Our results reveal the importance of IcsB-dependent N^ε-fatty acylation of the trafficking regulator Rab35 during bacterial invasion (Figures 3, 4, and 5). Our data using the Δ icsB mutant and the Rab35 lysine mutants in click-chemistry assays demonstrates the subversion of this GTPase through lysine N^ε-fatty acylation.

Weddle and Agaisse previously reported that IcsB is required for efficient cell-to-cell spread in HT-29 cells. They further showed that this phenotype was unrelated to the counteracting of LC3 recruitment on secondary BCVs, but their study did not further characterize the mechanistic links between IcsB, BCV escape, and cell-to-cell spread.⁴⁴ Here, we show that Rab35 and IcsB both promote efficient bacterial access to the host cytosol (Figure 6), and our plaque assay results suggest the same link between IcsB and efficient cell-to-cell spread. However, we could not fully resolve the mechanistic link between IcsB and intercellular motility because our attempts to complement our Δ icsB mutant in the plaque assays did not recover the plaque size to WT levels. Importantly, these strains showed full complementation of the Rab35 recruitment phenotype (Figure 3). We suggest that this is due to dysregulated *icsB* expression, resulting in fitness defects during long-time plaque formation assays.

In summary, the rapid disassembly of the *Shigella*-BCV is a distinct feature of this pathogen, different from cytosolic *Salmonella* that remains closely connected with their BCV remnants.^{45,46} The cytosol can be highly detrimental for the bacteria due to their targeting by host pathways, such as the autophagy machinery.⁴⁷ Furthermore, septins can target non-motile intracellular *Shigella*.¹⁵ Because the BCV membrane remnants are capable of bringing cellular complexes with antibacterial function into proximity to the entering bacteria, we suggest that the separation of both of them promotes the propagation of the pathogen.⁴⁸ Our study sheds light on the IcsB-mediated Rab35 subversion during *Shigella* invasion of colonic epithelial cells. Ultimately, a better understanding of host protein subversion during bacterial invasion can lead to the development of novel and more efficient therapeutic strategies against an array of deadly intracellular pathogens.

(C–E) Live-cell image analysis to simultaneously monitor the onset time of vacuolar rupture by measuring the time interval between entry foci formation and galectin-3 recruitment (C), the time of vacuolar disassembly (D), and the onset of bacterial motility (E). Although vacuolar damage is not perturbed in Rab35 KO cells, BCV-membrane disassembly is delayed. Red bars: median (n > 30 per condition, analyzed from 4 independent experiments). Statistical significance: multiple comparisons ANOVA tests. *p < 0.05, **p < 0.01, ***p < 0.001, ****p < 0.0001.

(F and G) Cell-to-cell spread of *Shigella* WT and *Shigella* Δ icsB mutant in a confluent epithelial monolayer. (F) An infection focus assay to measure cell-to-cell spread. Caco-2 cells were infected with *Shigella* WT dsRed or Δ icsB dsRed mutant. Staining nuclei with DRAQ5 (purple) and anti-*Shigella* LPS (green). Images are representative of 4 independent experiments. Scale bar, 100 μ m. (G) Area of infection focus was quantified using Fiji. Red bars: median (n > 90 per condition, analyzed from 3 independent experiments). Statistical significance: Mann-Whitney test, ****p < 0.0001.

Limitations of the study

It is important to note that our study has a number of limitations. The reprogramming of Rab35 by IcsB could be analyzed *in vitro* and at the cellular level during the early steps of *Shigella* invasion; however, assays that take into account a multicellular context and bacterial cell-to-cell spread are more difficult to interpret. Indeed, the *Shigella icsB* mutant used in such assays may show different fitness and may affect multiple host pathways that have not been the focus of our experiments. To fully recapitulate the pathophysiological context of the role of Rab35 reprogramming during *Shigella* infection, further *in vivo* experiments are necessary. Because we observed slight phenotypic differences in terms of timing or intensity of host protein recruitment at *Shigella* BCVs in different cellular models, it is possible that such differences have an impact on the infection outcome *in vivo*.

STAR★METHODS

Detailed methods are provided in the online version of this paper and include the following:

- **KEY RESOURCES TABLE**
- **RESOURCE AVAILABILITY**
 - Lead contact
 - Materials availability
 - Data and code availability
- **EXPERIMENTAL MODEL AND STUDY PARTICIPANT DETAILS**
 - Bacterial strains, cells, cell culture and infections
- **METHOD DETAILS**
 - Plasmids, site-directed mutagenesis and DNA extractions
 - DNA transfection
 - Time lapse live-cell widefield microscopy and image analysis
 - Time lapse live-cell confocal microscopy
 - Super-resolution microscopy (STED)
 - Western blot
 - Infection focus assay (*Shigella* cell-to-cell spread)
 - Immunofluorescence microscopy
 - In-gel fluorescence and click chemistry
- **QUANTIFICATION AND STATISTICAL ANALYSIS**

SUPPLEMENTAL INFORMATION

Supplemental information can be found online at <https://doi.org/10.1016/j.celrep.2024.114034>.

ACKNOWLEDGMENTS

We would like to thank the current and previous members of the DIHP unit for helpful discussion and feedback, especially Yuen Yan Chang. Also, we thank Bruno Goud, Claude Parsot, Armelle Phalipon, Philippe Sansonetti, Feng Shao, Guy Tran Van Nhieu, and John Rohde for sharing tools. The J.E. team has been supported by the Agence National pour la Recherche (grants: HBP sensing, PureMagRupture) and the European Commission (ERC-CoG Endosubvert). N.L.-M. has been funded by an EMBO short-term fellowship. G.M., D.D., and J.E. thank the “Region Ile de France” for the DIM-One-Health grant.

AUTHOR CONTRIBUTIONS

Conceptualization and project administration, N.M., N.L.-M., A.E., and J.E. Methodology and visualization, N.M., N.L.-M., A.L., M.G., C.V., and G.M. Investigation, N.M., N.L.-M., G.M., A.L., and C.V. Formal analysis, N.M., N.L.-M., and A.L. STED analysis, G.M. and D.D. Resources, C.V., K.K., L.S., A.E., and J.E. Writing – original draft, N.M., A.L., and J.E. Writing – review & editing, N.M., A.L., C.V., D.D., A.E., and J.E. Supervision, N.M., and J.E. Funding acquisition, G.M., D.D., A.E., and J.E. All of the authors discussed the results and commented on the manuscript.

DECLARATION OF INTERESTS

The authors declare no competing interests.

Received: December 13, 2022

Revised: November 12, 2023

Accepted: March 18, 2024

REFERENCES

1. Bajunaid, W., Haidar-Ahmad, N., Kottarampatel, A.H., Ourida Manigat, F., Silué, N., Tchagang, C.F., Tomaro, K., and Campbell-Valois, F.-X. (2020). The T3SS of *Shigella*: Expression, Structure, Function, and Role in Vacuole Escape. *Microorganisms* **8**, 1933. <https://doi.org/10.3390/microorganisms8121933>.
2. Chang, Y.-Y., Stévenin, V., Duchateau, M., Giai Gianetto, Q., Hourdel, V., Rodrigues, C.D., Matondo, M., Reiling, N., and Enninga, J. (2020). *Shigella* hijacks the exocyst to cluster macropinosomes for efficient vacuolar escape. *PLoS Pathog.* **16**, e1008822. <https://doi.org/10.1371/journal.ppat.1008822>.
3. Mellouk, N., and Enninga, J. (2016). Cytosolic Access of Intracellular Bacterial Pathogens: The *Shigella* Paradigm. *Front. Cell. Infect. Microbiol.* **6**, 35. <https://doi.org/10.3389/fcimb.2016.00035>.
4. Ray, K., Bobard, A., Danckaert, A., Paz-Haftel, I., Clair, C., Ehsani, S., Tang, C., Sansonetti, P., Tran, G.V.N., and Enninga, J. (2010). Tracking the dynamic interplay between bacterial and host factors during pathogen-induced vacuole rupture in real time. *Cell Microbiol.* **12**, 545–556. <https://doi.org/10.1111/j.1462-5822.2010.01428.x>.
5. Schnupf, P., and Sansonetti, P.J. (2019). *Shigella* Pathogenesis: New Insights through Advanced Methodologies. *Microbiol. Spectr.* **7**. <https://doi.org/10.1128/microbiolspec.BAI-0023-2019>.
6. Mellouk, N., Weiner, A., Aulner, N., Schmitt, C., Elbaum, M., Shorte, S.L., Danckaert, A., and Enninga, J. (2014). *Shigella* Subverts the Host Recycling Compartment to Rupture Its Vacuole. *Cell Host Microbe* **16**, 517–530. <https://doi.org/10.1016/j.chom.2014.09.005>.
7. Weiner, A., Mellouk, N., Lopez-Montero, N., Chang, Y.-Y., Souque, C., Schmitt, C., and Enninga, J. (2016). Macropinosomes are Key Players in Early *Shigella* Invasion and Vacuolar Escape in Epithelial Cells. *PLoS Pathog.* **12**, e1005602. <https://doi.org/10.1371/journal.ppat.1005602>.
8. López-Montero, N., and Enninga, J. (2018). Diverted recycling—*Shigella* subversion of Rabs. *Small GTPases* **9**, 365–374. <https://doi.org/10.1080/21541248.2016.1240494>.
9. Kayath, C.A., Hussey, S., El hajjami, N., Nagra, K., Philpott, D., and Allaoui, A. (2010). Escape of intracellular *Shigella* from autophagy requires binding to cholesterol through the type III effector. *Microb. Infect.* **12**, 956–966. <https://doi.org/10.1016/j.micinf.2010.06.006>.
10. Kühn, S., Bergqvist, J., Gil, M., Valenzuela, C., Barrio, L., Lebreton, S., Zurzolo, C., and Enninga, J. (2020). Actin Assembly around the *Shigella*-Containing Vacuole Promotes Successful Infection. *Cell Rep.* **31**, 107638. <https://doi.org/10.1016/j.celrep.2020.107638>.
11. Liu, W., Zhou, Y., Peng, T., Zhou, P., Ding, X., Li, Z., Zhong, H., Xu, Y., Chen, S., Hang, H.C., and Shao, F. (2018). Ne-fatty acylation of multiple membrane-associated proteins by *Shigella* IcsB effector to modulate

- host function. *Nat. Microbiol.* **3**, 996–1009. <https://doi.org/10.1038/s41564-018-0215-6>.
12. Ogawa, M., Yoshimori, T., Suzuki, T., Sagara, H., Mizushima, N., and Sasakawa, C. (2005). Escape of Intracellular Shigella from Autophagy. *Science* **307**, 727–731. <https://doi.org/10.1126/science.1106036>.
 13. Ogawa, M., Suzuki, T., Tatsuno, I., Abe, H., and Sasakawa, C. (2003). IcsB, secreted via the type III secretion system, is chaperoned by IpgA and required at the post-invasion stage of Shigella pathogenicity: The role of IcsB in Shigella pathogenicity. *Mol. Microbiol.* **48**, 913–931. <https://doi.org/10.1046/j.1365-2958.2003.03489.x>.
 14. Allaoui, A., Mounier, J., Prévost, M.C., Sansonetti, P.J., and Parsot, C. (1992). IcsB: a Shigella flexneri virulence gene necessary for the lysis of protrusions during intercellular spread. *Mol. Microbiol.* **6**, 1605–1616. <https://doi.org/10.1111/j.1365-2958.1992.tb00885.x>.
 15. Mostowy, S., Bonazzi, M., Hamon, M.A., Tham, T.N., Mallet, A., Lelek, M., Gouin, E., Demangel, C., Brosch, R., Zimmer, C., et al. (2010). Entrapment of Intracytosolic Bacteria by Septin Cage-like Structures. *Cell Host Microbe* **8**, 433–444. <https://doi.org/10.1016/j.chom.2010.10.009>.
 16. Stenmark, H. (2009). Rab GTPases as coordinators of vesicle traffic. *Nat. Rev. Mol. Cell Biol.* **10**, 513–525. <https://doi.org/10.1038/nrm2728>.
 17. Chavrier, P., Gorvel, J.-P., Stelzer, E., Simons, K., Gruenberg, J., and Zerial, M. (1991). Hypervariable C-terminal domain of rab proteins acts as a targeting signal 353, 4. <https://doi.org/10.1038/353769a0>.
 18. Escoll, P., Mondino, S., Rolando, M., and Buchrieser, C. (2016). Targeting of host organelles by pathogenic bacteria: a sophisticated subversion strategy. *Nat. Rev. Microbiol.* **14**, 5–19. <https://doi.org/10.1038/nrmicro.2015.1>.
 19. Chaîneau, M., Ioannou, M.S., and McPherson, P.S. (2013). Rab35: GEFs, GAPs and Effectors. *Traffic* **14**, 1109–1117. <https://doi.org/10.1111/tra.12096>.
 20. Klinkert, K., and Echard, A. (2016). Rab35 GTPase: A Central Regulator of Phosphoinositides and F-actin in Endocytic Recycling and Beyond. *Traffic* **17**, 1063–1077. <https://doi.org/10.1111/tra.12422>.
 21. Shaughnessy, R., and Echard, A. (2018). Rab35 GTPase and cancer: Linking membrane trafficking to tumorigenesis. *Traffic* **19**, 247–252. <https://doi.org/10.1111/tra.12546>.
 22. Li, F., Yi, L., Zhao, L., Itzen, A., Goody, R.S., and Wu, Y.-W. (2014). The role of the hypervariable C-terminal domain in Rab GTPases membrane targeting. *Proc. Natl. Acad. Sci. USA* **111**, 2572–2577. <https://doi.org/10.1073/pnas.1313655111>.
 23. Egami, Y., Fukuda, M., and Araki, N. (2011). Rab35 regulates phagosome formation through recruitment of ACAP2 in macrophages during FcγR-mediated phagocytosis. *J. Cell Sci.* **124**, 3557–3567. <https://doi.org/10.1242/jcs.083881>.
 24. Dambournet, D., Machicoane, M., Chesneau, L., Sachse, M., Rocancourt, M., El Marjou, A., Formstecher, E., Salomon, R., Goud, B., and Echard, A. (2011). Rab35 GTPase and OCRL phosphatase remodel lipids and F-actin for successful cytokinesis. *Nat. Cell Biol.* **13**, 981–988. <https://doi.org/10.1038/ncb2279>.
 25. Deng, W., Wang, Y., Gu, L., Duan, B., Cui, J., Zhang, Y., Chen, Y., Sun, S., Dong, J., and Du, J. (2016). MICAL1 controls cell invasive phenotype via regulating oxidative stress in breast cancer cells. *BMC Cancer* **16**, 489. <https://doi.org/10.1186/s12885-016-2553-1>.
 26. Klinkert, K., Rocancourt, M., Houdusse, A., and Echard, A. (2016). Rab35 GTPase couples cell division with initiation of epithelial apico-basal polarity and lumen opening. *Nat. Commun.* **7**, 11166. <https://doi.org/10.1038/ncomms11166>.
 27. Rahajeng, J., Giridharan, S.S.P., Cai, B., Naslavsky, N., and Caplan, S. (2012). MICAL-L1 is a tubular endosomal membrane hub that connects Rab35 and Arf6 with Rab8a. *Traffic* **13**, 82–93. <https://doi.org/10.1111/j.1600-0854.2011.01294.x>.
 28. Zhang, J., Fonovic, M., Suyama, K., Bogoy, M., and Scott, M.P. (2009). Rab35 controls actin bundling by recruiting fascin as an effector protein. *Science* **325**, 1250–1254. <https://doi.org/10.1126/science.1174921>.
 29. Goody, P.R., Heller, K., Oesterlin, L.K., Müller, M.P., Itzen, A., and Goody, R.S. (2012). Reversible phosphocholination of Rab proteins by Legionella pneumophila effector proteins: Rab phosphocholination and dephosphocholination. *EMBO J.* **31**, 1774–1784. <https://doi.org/10.1038/emboj.2012.16>.
 30. Mukherjee, S., Liu, X., Arasaki, K., McDonough, J., Galán, J.E., and Roy, C.R. (2011). Modulation of Rab GTPase function by a protein phosphocholine transferase. *Nature* **477**, 103–106. <https://doi.org/10.1038/nature10335>.
 31. Wandinger-Ness, A., and Zerial, M. (2014). Rab Proteins and the Compartmentalization of the Endosomal System. *Cold Spring Harbor Perspect. Biol.* **6**, a022616. <https://doi.org/10.1101/cshperspect.a022616>.
 32. Wang, M., Zhang, Y., Komaniecki, G.P., Lu, X., Cao, J., Zhang, M., Yu, T., Hou, D., Spiegelman, N.A., Yang, M., et al. (2022). Golgi stress induces SIRT2 to counteract Shigella infection via defatty-acylation. *Nat. Commun.* **13**, 4494. <https://doi.org/10.1038/s41467-022-32227-x>.
 33. Kallemeijn, W.W., Lanyon-Hogg, T., Panyain, N., Goya Grocin, A., Ciepla, P., Morales-Sanfrutos, J., and Tate, E.W. (2021). Proteome-wide analysis of protein lipidation using chemical probes: in-gel fluorescence visualization, identification and quantification of N-myristoylation, N- and S-acylation, O-cholesterylation, S-farnesylation and S-geranylgeranylation. *Nat. Protoc.* **16**, 5083–5122. <https://doi.org/10.1038/s41596-021-00601-6>.
 34. Allgood, S.C., Romero Dueñas, B.P., Noll, R.R., Pike, C., Lein, S., and Neunuebel, M.R. (2017). Legionella Effector AnkX Disrupts Host Cell Endocytic Recycling in a Phosphocholination-Dependent Manner. *Front. Cell. Infect. Microbiol.* **7**, 397. <https://doi.org/10.3389/fcimb.2017.00397>.
 35. Dikshit, N., Bist, P., Fenlon, S.N., Pulloor, N.K., Chua, C.E.L., Scidmore, M.A., Carlyon, J.A., Tang, B.L., Chen, S.L., and Sukumaran, B. (2015). Intracellular Uropathogenic E. coli Exploits Host Rab35 for Iron Acquisition and Survival within Urinary Bladder Cells. *PLoS Pathog.* **11**, e1005083. <https://doi.org/10.1371/journal.ppat.1005083>.
 36. Campbell-Valois, F.-X., and Pontier, S.M. (2016). Implications of Spatio-temporal Regulation of Shigella flexneri Type Three Secretion Activity on Effector Functions: Think Globally, Act Locally. *Front. Cell. Infect. Microbiol.* **6**, 28. <https://doi.org/10.3389/fcimb.2016.00028>.
 37. Ashida, H., and Sasakawa, C. (2015). Shigella IpaH Family Effectors as a Versatile Model for Studying Pathogenic Bacteria. *Front. Cell. Infect. Microbiol.* **5**, 100. <https://doi.org/10.3389/fcimb.2015.00100>.
 38. Li, H., Xu, H., Zhou, Y., Zhang, J., Long, C., Li, S., Chen, S., Zhou, J.-M., and Shao, F. (2007). The Phosphothreonine Lyase Activity of a Bacterial Type III Effector Family. *Science* **315**, 1000–1003. <https://doi.org/10.1126/science.1138960>.
 39. Li, Z., Liu, W., Fu, J., Cheng, S., Xu, Y., Wang, Z., Liu, X., Shi, X., Liu, Y., Qi, X., et al. (2021). Shigella evades pyroptosis by arginine ADP-ribosylation of caspase-11. *Nature* **599**, 290–295. <https://doi.org/10.1038/s41586-021-04020-1>.
 40. Burnaevskiy, N., Fox, T.G., Plymire, D.A., Ertelt, J.M., Weigele, B.A., Seylunin, A.S., Way, S.S., Patrie, S.M., and Alto, N.M. (2013). Proteolytic elimination of N-myristoyl modifications by the Shigella virulence factor IpaJ. *Nature* **496**, 106–109. <https://doi.org/10.1038/nature12004>.
 41. Sanada, T., Kim, M., Mimuro, H., Suzuki, M., Ogawa, M., Oyama, A., Ashida, H., Kobayashi, T., Koyama, T., Nagai, S., et al. (2012). The Shigella flexneri effector OspI deamidates UBC13 to dampen the inflammatory response. *Nature* **483**, 623–626. <https://doi.org/10.1038/nature10894>.
 42. Zhang, L., Ding, X., Cui, J., Xu, H., Chen, J., Gong, Y.-N., Hu, L., Zhou, Y., Ge, J., Lu, Q., et al. (2011). Cysteine methylation disrupts ubiquitin-chain sensing in NF-κB activation. *Nature* **481**, 204–208. <https://doi.org/10.1038/nature10690>.
 43. Zhang, Y., Mühlen, S., Oates, C.V., Pearson, J.S., and Hartland, E.L. (2016). Identification of a Distinct Substrate-binding Domain in the Bacterial Cysteine Methyltransferase Effectors NieE and OspZ. *J. Biol. Chem.* **291**, 20149–20162. <https://doi.org/10.1074/jbc.M116.734079>.

44. Weddle, E., and Agaisse, H. (2018). Spatial, Temporal, and Functional Assessment of LC3-Dependent Autophagy in *Shigella flexneri* Dissemination. *Infect. Immun.* *86*, e001344–18. <https://doi.org/10.1128/IAI.00134-18>.
45. Fredlund, J., Santos, J.C., Stévenin, V., Weiner, A., Latour-Lambert, P., Rechav, K., Mallet, A., Krijnse-Locker, J., Elbaum, M., and Enninga, J. (2018). The entry of *Salmonella* in a distinct tight compartment revealed at high temporal and ultrastructural resolution. *Cell Microbiol.* *20*, e12816. <https://doi.org/10.1111/cmi.12816>.
46. Stévenin, V., Chang, Y.-Y., Le Toquin, Y., Duchateau, M., Gianetto, Q.G., Luk, C.H., Salles, A., Sohst, V., Matondo, M., Reiling, N., and Enninga, J. (2019). Dynamic Growth and Shrinkage of the *Salmonella*-Containing Vacuole Determines the Intracellular Pathogen Niche. *Cell Rep.* *29*, 3958–3973.e7. <https://doi.org/10.1016/j.celrep.2019.11.049>.
47. Noad, J., von der Malsburg, A., Pathe, C., Michel, M.A., Komander, D., and Randow, F. (2017). LUBAC-synthesized linear ubiquitin chains restrict cytosol-invading bacteria by activating autophagy and NF- κ B. *Nat. Microbiol.* *2*, 17063. <https://doi.org/10.1038/nmicrobiol.2017.63>.
48. Thurston, T.L.M., Wandel, M.P., von Muhlinen, N., Foeglein, Á., and Randow, F. (2012). Galectin 8 targets damaged vesicles for autophagy to defend cells against bacterial invasion. *Nature* *482*, 414–418. <https://doi.org/10.1038/nature10744>.
49. Onodera, N.T., Ryu, J., Durbic, T., Nislow, C., Archibald, J.M., and Rohde, J.R. (2012). Genome sequence of *Shigella flexneri* serotype 5a strain M90T Sm. *J. Bacteriol.* *194*, 3022. <https://doi.org/10.1128/JB.00393-12>.
50. Rathman, M., Jouirhi, N., Allaoui, A., Sansonetti, P., Parsot, C., and Tran Van Nhieu, G. (2000). The development of a FACS-based strategy for the isolation of *Shigella flexneri* mutants that are deficient in intercellular spread. *Mol. Microbiol.* *35*, 974–990. <https://doi.org/10.1046/j.1365-2958.2000.01770.x>.
51. Paz, I., Sachse, M., Dupont, N., Mounier, J., Cederfur, C., Enninga, J., Lefler, H., Poirier, F., Prevost, M.C., Lafont, F., and Sansonetti, P. (2010). Galectin-3, a marker for vacuole lysis by invasive pathogens. *Cell Microbiol.* *12*, 530–544. <https://doi.org/10.1111/j.1462-5822.2009.01415.x>.
52. Ehsani, S., Santos, J.C., Rodrigues, C.D., Henriques, R., Audry, L., Zimmer, C., Sansonetti, P., Tran Van Nhieu, G., and Enninga, J. (2012). Hierarchies of host factor dynamics at the entry site of *Shigella flexneri* during host cell invasion. *Infect. Immun.* *80*, 2548–2557. <https://doi.org/10.1128/IAI.06391-11>.
53. Cauvin, C., Rosendale, M., Gupta-Rossi, N., Rocancourt, M., Larraufie, P., Salomon, R., Perrais, D., and Echard, A. (2016). Rab35 GTPase Triggers Switch-like Recruitment of the Lowe Syndrome Lipid Phosphatase OCRL on Newborn Endosomes. *Curr. Biol.* *26*, 120–128. <https://doi.org/10.1016/j.cub.2015.11.040>.
54. Labigne-Roussel, A.F., Lark, D., Schoolnik, G., and Falkow, S. (1984). Cloning and expression of an afimbrial adhesin (AFA-I) responsible for P blood group-independent, mannose-resistant hemagglutination from a pyelonephritic *Escherichia coli* strain. *Infect. Immun.* *46*, 251–259. <https://doi.org/10.1128/IAI.46.1.251-259.1984>.
55. Sidik, S., Kottwitz, H., Benjamin, J., Ryu, J., Jarrar, A., Garduno, R., and Rohde, J.R. (2014). A *Shigella flexneri* Virulence Plasmid Encoded Factor Controls Production of Outer Membrane Vesicles. *G3 (Bethesda)*. *4*, 2493–2503. <https://doi.org/10.1534/g3.114.014381>.
56. Parsot, C., Ménard, R., Gounon, P., and Sansonetti, P.J. (1995). Enhanced secretion through the *Shigella flexneri* Mxi-Spa translocon leads to assembly of extracellular proteins into macromolecular structures. *Mol. Microbiol.* *16*, 291–300. <https://doi.org/10.1111/j.1365-2958.1995.tb02301.x>.
57. Chesneau, L., Dambournet, D., Machicoane, M., Kouranti, I., Fukuda, M., Goud, B., and Echard, A. (2012). An ARF6/Rab35 GTPase Cascade for Endocytic Recycling and Successful Cytokinesis. *Curr. Biol.* *22*, 147–153. <https://doi.org/10.1016/j.cub.2011.11.058>.
58. Schindelin, J., Arganda-Carreras, I., Frise, E., Kaynig, V., Longair, M., Pietzsch, T., Preibisch, S., Rueden, C., Saalfeld, S., Schmid, B., et al. (2012). Fiji: an open-source platform for biological-image analysis. *Nat. Methods* *9*, 676–682. <https://doi.org/10.1038/nmeth.2019>.

STAR★METHODS

KEY RESOURCES TABLE

REAGENT or RESOURCE	SOURCE	IDENTIFIER
Antibodies		
Rabbit anti-GFP	Invitrogen	#A6455
Rat anti-Galectin-3	Novus biologicals	#NBP1-43313
Goat anti-rabbit Alexa 488	Invitrogen	#A11034
Goat anti-rabbit Alexa 647	Invitrogen	#A32733
Goat anti-rabbit StarOrange	Abberior	#STORANGE-1002
Goat anti-rat Atto647N	Rockland	#612-156-120
monoclonal mouse anti- β -actin	Sigma	#A5316
polyclonal rabbit anti-Rab35	ProteinTech	#11329-2-AP
Goat anti-mouse HRP	Bio-Rad	#1706516
Goat anti-rabbit HRP	Bio-Rad	#1706515
Rabbit anti-Flag	Proteintech	#20543-1-AP
Bacterial and virus strains		
<i>Shigella flexneri</i> (WT) 5a M90T-Sm, pWR100 (GenBank #AL391753.1)	Philippe Sansonetti John R. Rohde (Onodera et al. ⁴⁹)	GenBank#CM001474.1
<i>S. flexneri</i> (WT) expressing Afa-I (afaE gene) from <i>E. coli</i>	John R. Rohde	N/A
<i>S. flexneri</i> (WT) expressing dsRed and AfaI	Yuen-Yan Chang	N/A
<i>S. flexneri</i> (WT) expressing BFP	This work	N/A
<i>S. flexneri</i> (Δ icsB) expressing AfaI	This work	N/A
<i>S. flexneri</i> (Δ icsB complemented) expressing AfaI, IcsB and IpgA	This work	N/A
<i>S. flexneri</i> Δ icsB-2 (FXS299)	Claude Parsot (Rathman et al. ⁵⁰)	N/A
<i>S. flexneri</i> Δ icsB-2 complemented	Claude Parsot (Allaoui et al. ¹⁴)	N/A
<i>S. flexneri</i> M90T (WT) expressing mCherry and Afa-I (<i>E. coli</i> pIL22)	Guy Tran Van Nhieu	N/A
<i>Escherichia coli</i> InvA (<i>Yersinia</i> invasin A)	Guy Tran Van Nhieu	N/A
<i>Escherichia coli</i> DH5 α	Thermo Fisher Scientific	#18265017
Chemicals, peptides, and recombinant proteins		
X-tremeGENE™ 9 DNA transfection reagent	Roche	#6365779001
X-tremeGENE™ HP DNA transfection reagent	Roche	#6366244001
Lipofectamine RNAiMAX	Invitrogen	#13778030
DAPI	Thermo Fisher Scientific	#D1306
Gentamicin	Wisent	#400-130-IG
Paraformaldehyde 16%	Electron Microscopy Sciences	#15710
Ampicillin	Sigma-Aldrich	#A9393
Kanamycin	Sigma-Aldrich	#K1377
Poly-L-lysine	Sigma-Aldrich	#P4707
Dulbecco's Modified Eagle's Medium, High Glucose, GlutaMax	Thermo Fisher Scientific	#10566016
Fetal Bovine Serum	Sigma-Aldrich	#F7524
DPBS	Thermo Fisher Scientific	#14190144
MEM Non-Essential Amino Acids Solution	Thermo Fisher Scientific	#11140050
HEPES	Thermo Fisher Scientific	#15630080
0.05% Trypsin-EDTA	Thermo Fisher Scientific	#25300054

(Continued on next page)

REAGENT or RESOURCE	SOURCE	IDENTIFIER
ProLong Gold Antifade Mountant	ThermoFisher Scientific	#P10144
Complete Protease Inhibitor	Roche	#11836170001
4-12% Bis-Tris NuPAGE polyacrylamide gel	Thermo Fisher Scientific	# NP0335BOX
10% Bis-Tris NuPAGE polyacrylamide gel	Thermo Fisher Scientific	#N0316BOX
Micro BCA™ Protein Assay Kit	Thermo Fisher Scientific	#23235
PVDF membrane	Bio-Rad	#1620177
Radio Immune Precipitation Assay Buffer	ThermoFisher Scientific	#89901
SuperSignal™ West Pico Chemiluminescent Substrate	Thermo Scientific	#34080
Q5 site-directed mutagenesis kit	New England Biolabs	#E0554S
DRAQ5	Invitrogen	#65088096
17-Octadecynoic acid	Cayman chemicals	#90270
SDS	Sigma Aldrich	#05030
Triton X-100	Sigma Aldrich	23,472-9
Azide fluor 545	Sigma Aldrich	760757
CuSO4	Honeywell Fluka	35185
TCEP, HCl	Calbiochem	51805-45-9
TBTA	Cayman Chemicals	18816
EDTA	Invitrogen	15575-038
Laemmli buffer	Bio-Rad	161-0747
Beta mercaptoethanol	Sigma-Aldrich	M7154
Hydroxylamine	Sigma-Aldrich	438227
Experimental models: cell lines		
HeLa Human cervix carcinoma epithelial cell line clone CCL-2	ATCC	#11033106
Caco-2 TC7 cells	Philippe Sansonetti	N/A
HCT-116 intestinal cells clone CCL-247	ATCC	#ATCC-CCL-247
HEK 293T cells clone 17	ATCC	#ATCC-CRL-11268
Recombinant DNA		
GFP-galectin-3	Paz et al. ⁵¹	N/A
mOrange-Galectin3	Ehsani et al. ⁵²	N/A
GFP-Rab35	Cauvin et al. ⁵³	N/A
RFP-Rab35	Cauvin et al. ⁵³	N/A
EPI64B-mcherry	Cauvin et al. ⁵³	N/A
GFP-Rab5	Bruno Goud	N/A
pCS2-3HA-IcsB	Feng Shao (Liu et al. ¹¹)	N/A
pCS2-3HA-IcsB-C306A	Feng Shao (Liu et al. ¹¹)	N/A
pENTR-Rab35-Flag	Arnaud Echard (Cauvin et al. ⁵³)	NA
pENTR-Rab35-Flag-3KR	This work	N/A
Software and algorithms		
FIJI	NIH	https://fiji.sc https://imagej.net/ImageJ
Volocity 6.3 PerkinElmer	PerkinElmer	N/A
NIS-Elements Microscope Imaging Software	Nikon	N/A
GraphPad Prism	GraphPad Software v9.0, La Jolla, USA	https://www.graphpad.com/
Excel	Microsoft	N/A
ICY	Institut Pasteur	http://icy.bioimageanalysis.org/

(Continued on next page)

Continued

REAGENT or RESOURCE	SOURCE	IDENTIFIER
Other		
Perkin Elmer UltraView spinning disk confocal microscope equipped with the followings:	Perkin Elmer	N/A
60 × /1.3 oil objective	Nikon	N/A
PSU C910-50 camera	Hamamatsu	N/A
Inverted widefield microscope equipped with the followings:	Nikon	N/A
20x/0.5NA air objective	Nikon	N/A
CoolSnap2 camera	Roeper Scientific	N/A
Deltavision epifluorescence microscope	GE Healthcare	N/A
Typhoon FLA 9000	GE Healthcare	N/A
96-well cell culture microplates with clear flat bottom	Greiner Bio One International	#655090
Precision cover glasses thickness No. 1.5H	Marienfeld Superior	#0117580
35 mm glass bottom μ -Dishes (high-border)	Ibidi	#81158
8-well glass-bottom chambers	Ibidi	#80807-90
35 mm glass bottom μ -Dishes (low-border)	Ibidi	#80137
T25 flasks	Falcon	#009026
T75 flasks	Falcon	#009076
10cm dishes	Corning	#353003

RESOURCE AVAILABILITY

Lead contact

Further information and requests for resources and reagents should be directed to and will be fulfilled by the lead contact, Jost Enninga (jost.enninga@pasteur.fr).

Materials availability

This study did not generate new unique reagents.

Data and code availability

- Original data are available from the [lead contact](#) on request.
- This paper does not report original code.
- Any additional information required to reanalyze the data is available from the [lead contact](#) on request.

EXPERIMENTAL MODEL AND STUDY PARTICIPANT DETAILS

Bacterial strains, cells, cell culture and infections

Every *Shigella flexneri* serotype M90T (shortly *Shigella*) strain used in this work expressed the adhesin Afal to promote bacterial adhesion to the host cell,⁵⁴ except the *Shigella* WT BFP strain. Wild-type (WT) Afal dsRed (Yuen-Yan Chang), wild-type Afal, Δ *icsB* Afal (deficient in *IcsB*),⁵⁵ and the complemented Δ *icsB/icsB* Afal strains were grown in tryptic casein soy broth (TCSB) at 37°C or cultured on TCSB agar containing 0.01% of Congo Red to select for clones with a functional T3SS system.⁵⁶ The growth medium was systematically supplemented with ampicillin (50 μ g/mL). *E. coli* InvA strain containing the *Yersinia* invasin A was grown at 37°C in lysogeny broth (LB) media supplemented with ampicillin (100 μ g/mL).¹⁴ *E. coli* DH5 α and derivatives were grown at 37°C in LB supplemented either with ampicillin (100 μ g/mL) or kanamycin (50 μ g/mL), depending on the resistance of the corresponding plasmid.

Human intestinal epithelial Caco-2 cells (clone TC7 from the Sansonetti lab), HCT-116 intestinal cells (ATCC), Human epithelial HeLa cells (clone CCLX2 from ATCC), and HeLa cells expressing endogenously GFP-tagged Rab35⁵³ were cultured in Dulbecco's modified Eagle's medium (DMEM) supplemented with 10% inactivated fetal bovine serum (FBS) at 37°C, 5% CO₂. All cells of this study were passaged when their confluence reached 80%. For generating the Rab35 HeLa knockout cells (KO), we used the pX330-U6-Chimeric_BB-CBh-hSpCas9 plasmid (Addgene, plasmid # 42230). We chose the sequence 5' tgctcatcatcgcgacag 3' to allow the synthesis of gRNAs targeting human Rab35 Exon 1. Out of the clones we obtained, clone No.2 was tested for absence of Rab35 expression and taken for our studies. Furthermore, the KO cells were functionally characterized.

For infection experiments, overnight bacterial cultures were inoculated at a 1:100 dilution in TCSB supplemented with the appropriate antibiotics depending on the strains (and 2 mM IPTG for complementation assays), and grown to an optical density between 0.4 and 0.6 at 600 nm (OD₆₀₀). For time lapse imaging experiments, prior to infection, bacteria were washed twice with EM buffer (120 mM NaCl, 7 mM KCl, 1.8 mM CaCl₂, 0.8 mM MgCl₂, 5 mM glucose, 25 mM HEPES, pH 7.3) and finally diluted in EM buffer to reach a MOI of 20. Because *Shigella* WT BFP does not express Afal, it was coated with poly-L-lysine (10 μg/mL) for 10 min at 37°C and washed twice in EM buffer prior to dilution to reach a MOI of 50. In 8 well-lbidi chambers (clinisciences), 100 μL per well of the diluted bacterial suspension was added to the cells.

METHOD DETAILS

Plasmids, site-directed mutagenesis and DNA extractions

The Galectin-3 mOrange/GFP,⁴ GFP-Rab35, RFP-Rab35, EPI64B-mcherry,⁵⁷ GFP-Rab5 (kind gift from Bruno Goud) plasmids have been described previously. The mutated GFP-Rab35 plasmids where one or several lysins were replaced by arginines namely GFP-Rab35-K195R, GFP-Rab35-2KR (K197R, K198R) and GFP-Rab35-3KR (K195R, K197R, K198R) were generated using the Q5 site-directed mutagenesis kit (New England Biolabs, #E0554S). Mutagenesis primers were Forward_Rab35-K195R (gaagaacagtagac-gaaagaaacg), Reverse_Rab35-K195R (gtgagcttcaccacatcg), Forward_Rab35-2KR (cagtaaacgaaggagagcgtgctgct), Reverse_Rab35-2KR (ttctctgtagcttcacc), Forward_Rab35-3KR (aggagagcgtgctgctaagacc), Reverse_Rab35-3KR (tcgtctactgttctctgtagcttcac). Following the manufacturer instructions, the elongation time of PCRs was set at 4 min, and the temperatures of annealing (Ta) were adjusted depending on the construct: Ta Rab35-K195R 60°C; Ta Rab35-2KR 62.1°C; Ta Rab35-3KR 65°C. After PCR and digestion of the template plasmid (using the kit products and instructions), constructs were transformed in DH5α *E. coli* cells, and transformants were selected on LB agar supplemented with ampicillin (50 μg/mL). DNA plasmids were extracted using either NucleoSpin Plasmid Transfection-grade or NucleoBond Xtra Maxi Plus kit (Macherey-Nagel). All plasmids were verified by sequencing.

pAfa1-*icsB* was generated by introducing XhoI and NotI sites in the pBR322-Afa1 plasmid. Then, the *icsB* gene was PCR amplified using the Phusion Plus DNA Polymerase (New England Biolabs) from the pUC8*icsB-igpA* plasmid from Claude Parsot, using primers ipgA_NotI (aattaaGCGGCCGCTtagtctcactctgaagtgtgttgcaatgg) and icsB_XhoI (ttaattCTCGAGtgagtagctcactcattagcacc). Vector and PCR product were digested using XhoI and NotI (New England Biolabs) and ligated using T4 DNA Ligase (New England Biolabs), according to the manufacturer instructions. Competent DH5α were transformed with the ligation product and selected in LB supplemented with ampicillin. Colonies were selected and used for miniprep purification of the product. The insertion was corroborated by digestion of the recombinant plasmids and one of the clones selected was used to transform *S. flexneri* M90T Δ*icsB*.

The pGG2 TagBFP plasmid was generated by replacing the dsRed cassette of pGG2 dsRed by a TagBFP fluorescent cassette. Briefly, the *tagBFP* gene was PCR amplified from the pBR322 TagBFP plasmid (lab collection) using Q5 High-Fidelity DNA Polymerase (NEB #M0491S) with: Forward_TagBFP (5'aattaacatgatgagcgag ctgattaaggag3') and Reverse_TagBFP (5'aattaagctagcttaattaagc ttgtgcccag3') primers with an elongation time of 30 s and Ta of 70°C. pGG2 dsRed Vector and PCR products were digested with NdeI and NheI and the digestion products were ligated using T4 DNA ligase (NEB #M0202S) following the manufacturer's protocol. Competent *E. coli* DH5α were transformed with the ligation product and transformants selected on LB + ampicillin (50 μg/mL) agar plates. DNA plasmids were extracted from positive clones by miniprep and checked by gel migration before transformation into *Shigella* M90T.

DNA transfection

For time lapse microscopy experiments, Caco-2 TC7 and HeLa cells were seeded into 8 well (200 μL) lbidi chambers at a density of 10,000 cells per well 24 h prior to transfection. The cells were then transfected with the desired plasmid(s), using respectively X-tremeGENE HP or X-tremeGENE 9 reagents (Roche) for 24 or 48 h. For Caco-2 TC7 cells, the volume of X-tremeGENE HP (ratio 4:1 to DNA amount) was added to a mix of DNA plasmids in Opti-MEM and was then incubated at room temperature (RT) for 15 min before transfection. For HeLa cells, DNA plasmids were directly added on a mix of X-tremeGENE 9 (ratio 3:1 to DNA amount) and Opti-MEM, before incubation for 15 min at RT. Meanwhile, fresh culture media was provided to the cells, and 15 μL of the transfection mix was added per well.

Time lapse live-cell widefield microscopy and image analysis

Infected cells in EM buffer were imaged at 37°C using a DeltaVision Elite (GE Healthcare) widefield microscope using a 60X/1.42 NA oil objective. Cells were imaged every minute for 90 min, on a range of 8 μm, with a section spacing of 0.3 μm in the Z dimension and using a piezo control and the UltimateFocus module to keep the plane in focus. TRITC and FITC excitation and emission filters were used. Movies were subsequently deconvolved using the integrated deconvolution software of the DeltaVision microscope. Image analysis was systematically performed using Fiji (<http://fiji.sc>).⁵⁸ For Rab35 recruitment at the BCV, the analysis was performed on sum Z-projections of 5 Z slices englobing the corresponding bacterium. The fluorescence intensity in the green channel was then measured along the BCV, at 7 points at least and separated by a distance of 0.109 μm. The average intensity of the BCV was then computed using Excel. This process was also performed on 3 different areas of the host cell plasma membrane in order to estimate its mean fluorescence. Finally, the ratio between the mean fluorescence of GFP-Rab35 at the BCV and the mean fluorescence of GFP-Rab35 at the cell plasma membrane was computed for each internalized bacterium, either at the frame preceding the BCV rupture (Galectin-3-mOrange recruitment) or at the frame where the BCV was considered the most fluorescent. Live imaging of HeLa cells (WT or Rab35 KO) co-transfected with GFP-Rab35 and Galectin-3-mOrange and infected with *Shigella* WT were

analyzed as follow: (i) bacterial entry foci formation is the time when bacteria triggers host membrane ruffles, (ii) onset of vacuolar rupture is the time when galectin-3 appears around the BCV and (iii) time span of BCV disassembly is the time between complete BCV membrane disassembly and first appearance of galectin-3 around the BCV.

Time lapse live-cell confocal microscopy

Infected cells in EM buffer were imaged at 37°C using a PerkinElmer Ultra-View spinning disc confocal microscope, with a 40X/1.3 N.A. oil objective. Cells were imaged every minute for 90 min, on a range of 8 μm, with a section spacing of 0.3 μm in the Z dimension and using a piezo control and the Perfect Focus System (PFS) to keep the plane in focus. BFP, TRITC and FITC excitation and emission filters were used.

Super-resolution microscopy (STED)

For STED experiments, Caco-2 TC7 were seeded into 12 wells (1 mL) plates onto high precision cover glasses (Marienfeld 18mm No. 1.5H, #0117580) at a density of 30,000 cells per well 24 h prior to DNA transfection. The cells were then transfected with the GFP-Rab35 plasmid using X-tremeGENE HP for 24 h. Once the transfected cells were 80% confluent, they were infected (following the infection protocol described above) and incubated for 30 min at 37°C, 5% CO₂. Cells were fixed with 4% PFA in DPBS for 15 min and blocked for 1 h with 5% goat serum and 0.05% saponin in DPBS (SS-PBS) at room temperature. Subsequently, cells were incubated overnight at 4°C with the primary antibodies Rabbit anti-GFP (Invitrogen, #A6455) and Rat anti-Galectin-3 (Novus biologicals, #NBP1-43313) diluted at 1:100 in SS-PBS. Cells were washed 3 times in DPBS for 5 min and then incubated for 1 h at room temperature with the secondary antibodies goat anti-rabbit StarOrange (Abberior, #STORANGE-1002) and goat anti-rat Atto647N (Rockland, #612-156-120) diluted at 1:200 in SS-PBS. Cells were then washed 3 times in DPBS for 5 min and mounted with Mowiol containing DABCO medium on glass slides. Cells were imaged with a Stimulated Emission Depletion (STED) fluorescence microscope (expert line - Abberior Instruments) using an Olympus 100X/1.4 NA oil objective lens and a 775nm STED Laser line. STED Images were analyzed using Fiji.⁵⁸ The region of interest along the membrane was first straighten. Then, Gaussian fits of all the fluorescence intensity profiles of Rab35 across the membrane were independently shifted in order to be centered on the exact same transverse position. Gaussian fits of the fluorescence intensity profiles of Galectin-3 were subsequently shifted by the same amount as for the alignment of the Rab35 fits. Relevant profiles of Galectin-3 were selected by imposing a lower threshold on the maxima of the Gaussian fits and an upper threshold on their widths. From the selected Galectin-3 profiles and Rab35 profiles, average profiles were computed to estimate the distance between the average positions. As well, the average of distances (in absolute values) between Rab35 and Galectin-3 distributions, over the selected positions along the membrane was calculated.

Western blot

Total cell lysates were collected using ice-cold Radio Immune Precipitation Assay Buffer (RIPA: 150 mM sodium chloride, 1% NP-40, 1% sodium deoxycholate, 0.1% SDS (sodium dodecyl sulfate), 25 mM Tris-HCl, pH 7.6) (ThermoFisher Scientific, #89901) supplemented with a cocktail of protease inhibitor (Roche, #11873580001). Upon incubation for 15 min on a rotating wheel at 4°C, cell debris were pelleted by spinning at 16,000 g for 15 min at 4°C. Protein concentrations were determined using a BCA protein assay kit (Pierce, #23225). Protein lysates containing 20 μg of total protein were loaded onto 4–12% Bis-Tris NuPAGE polyacrylamide gel (ThermoFisher Scientific, #NP0335BOX). Proteins were wet-transferred to an activated PVDF membrane (Bio-Rad, #1620177) for 1h30 at 100 V. Membranes were then blocked with 5% fat-free milk in TBS-T (Tris-buffered saline: 20 mM Tris, pH 7.5, 150 mM NaCl, 0.1% Tween 20) for 1 h at room temperature, and subsequently incubated overnight at 4°C with the primary antibodies diluted at 1:10000 (monoclonal mouse anti-β-actin, Sigma, #A5316) or 1:1000 (polyclonal rabbit anti-Rab35, ProteinTech, #11329-2-AP) in TBS-T supplemented with 5% fat-free milk. Membranes were washed 3 times in TBS-T for 5 min and then incubated for 1 h at room temperature with the secondary antibodies conjugated with HRP diluted at 1:10,000 (Goat anti-mouse HRP, Bio-Rad #1706516) or at 1:5000 (Goat anti-rabbit HRP, Bio-Rad #1706515) in TBS-T supplemented with 5% fat-free milk. Membranes were then washed 3 times in TBS-T for 5 min and revealed with the SuperSignal West PicoPlus chemiluminescent substrate (Thermo Scientific, #34577). Chemiluminescence images were acquired using a Chemidoc imager (BioRad).

Infection focus assay (*Shigella* cell-to-cell spread)

Caco-2 cells were plated at 10,000 cells per well in 96-well plate (Greiner bio-one, #655090). After 24 h, a fully confluent monolayer of Caco-2 cells was infected with *Shigella* WT or Δ *icsB* at an MOI of 0.05 in pre-warmed DMEM medium at 37°C, 5% CO₂. At 60 min post-infection, all cells were washed three times with PBS⁺ and cultured in DMEM medium containing 10% FBS and 50 μg mL⁻¹ gentamicin (Wisent, #400-130-IG). At 18 h post-infection, cells were fixed with 4% PFA and counterstained with rabbit anti-*Shigella* LPS (Gift from P. Sansonetti and A. Phalipon) and goat anti-rabbit Alexa Fluor 488 (Thermo scientific, #A11034) and DRAQ5 DNA dye (Invitrogen, #65088096), and imaged on a spinning disk confocal scan head equipped with a ×20 objective. The area of infection focus was quantified using Fiji.

Immunofluorescence microscopy

Caco-2 cells were plated at 10,000 cells per well in 96-well plate (Greiner bio-one, #655090). After 24 h, the cells were then co-transfected with the Galectin-3-GFP and Flag-Rab35 plasmids using X-tremeGENE HP for 48 h. Cells were fixed with 4% PFA in DPBS for

15 min and blocked for 1 h with 10% goat serum and 0.05% saponin in DPBS (SS-PBS) at room temperature. Subsequently, cells were incubated for 45 min at room temperature with the primary antibody Rabbit anti-flag (Proteintech, #20543-1-AP) diluted at 1:100 in SS-PBS. Cells were washed 3 times in DPBS for 5 min and then incubated for 30 min at room temperature with the secondary antibody goat anti-rabbit Alexa 647 (Invitrogen, #A32733) diluted at 1:200 and DRAQ5 DNA dye diluted at 1:500 (Invitrogen, #65088096) in SS-PBS. Cells were then washed 3 times in DPBS for 5 min. Cells were imaged using a spinning disk confocal scan head equipped with a $\times 60/1.3$ NA water objective on a range of 8 μm , with a section spacing of 0.3 μm in the Z dimension.

In-gel fluorescence and click chemistry

HEK 293T cells were seeded at 2×10^6 per 10cm diameter cell culture dishes (Falcon, #353003), in 10mL DMEM +10% FBS and incubated for two days at 37°C, 5%CO₂. Once reaching 70–80% confluence the cells were transfected with pENTR-Rab35-Flag, pENTR-Rab35-3KR-Flag, pCS2-3HA-IcsB or pCS2-3HA-IcsB-C306A (both kindly gifted by Feng Shao). Transfections were performed using OPTI-MEM (Gibco #31985-062) and Xtremegene9 (Sigma Aldrich, #063657790001), according to the manufacturer instructions using 5 μg DNA per dish. Cells were incubated for 6h at 37°C, 5% CO₂ and then, the media was replaced with 10mL DMEM +10% FBS supplemented with 50 μM 17-Octadecenoic acid (Cayman Chemicals, #90270) diluted in DMSO. The control dishes received DMEM +10% FBS supplemented with the same concentration of DMSO as the other conditions. Cells were then incubated at 37°C, 5% CO₂. 18h after the metabolic labeling, the plates were washed once with ice-cold PBS and the cells were lysed with 500 μL lysis buffer per condition (0.1% SDS (Sigma, #05030), 1% Triton X-100 (Sigma, #23,472-9), diluted in PBS, supplemented with a cocktail of protease inhibitor (Roche, #11873580001)). The obtained lysates were incubated on a rotating wheel for 30 min at 4°C and clarified by centrifugation at 15000rpm and recovery of the supernatant. This fraction was processed with a Chromotek flag-trap kit (#ffa) following the protocol of the manufacturer. Briefly, beads were equilibrated in 1000 μL ice-cold Dilution buffer (10 mM Tris/Cl pH 7.5, 150 mM NaCl, 0.5 mM EDTA) and sedimented by centrifugation at 2500g for 5 min at 4°C. The supernatant was discarded, and the beads resuspended in the clarified lysate obtained previously. The samples were then incubated at 4°C for 1h in a rotating wheel and subsequently centrifuged at 2500g for 5 min at 4°C and resuspended in 1000 μL ice-cold wash buffer (20 mM Tris/Cl pH 7.5, 150 mM NaCl), and sedimented again with the same parameters. In total beads were washed three times, and the supernatant was saved after each wash. After the last washing step of the flag-trap kit, beads were resuspended in 100 μL PBS and the bio-orthogonal tag functionalization was performed directly on the beads. For this, 6 μL click mix (1 μL 10mM azide fluor 545 (Sigma Aldrich, #760757), 2 μL 50mM CuSO₄, 2 μL 50mM TCEP (Calbiochem, #51805-45-9) and 1 μL 10mM TBTA (Cayman chemicals, #18816)) was added and the sample incubated for 1h at room temperature, on a vortex spinner (700rpm). The reaction was stopped by adding EDTA at a final concentration of 5mM. Samples were finally resuspended in Laemmli buffer (Bio-Rad, #1610737) with beta mercaptoethanol (Bio-Rad, #1610710), denatured at 95°C for 10min, loaded in a NuPAGE 10% Bis-Tris gel (#N0316BOX) and run at 120V for 1h30. The gel was then washed in water and imaged in a Typhoon FLA 9000, at a 100 μm resolution, TAMRA filters. The gel was then transferred to a PVDF membrane (Bio-Rad, #1620177) and processed for western-blotting, using a Rabbit anti-flag (Proteintech, #20543-1-AP) primary antibody at a 1/2000 dilution and an HRP Goat anti-Rabbit (BioRad, #1706515) secondary antibody, Supersignal West Pico chemiluminescence substrate (Thermoscientific, #34080) was used for detection.

QUANTIFICATION AND STATISTICAL ANALYSIS

Statistical analyses were performed in GraphPad Prism v9. Statistical significance was determined using a two-tailed Student's *t* test (Mann-Whitney) or a one-way ANOVA (Kruskal-Wallis) followed by Dunnett's multiple comparisons test. (ns) not significant, $p < 0.05$ was considered as significant: * $p < 0.05$, ** $p < 0.01$, *** $p < 0.001$, **** $p < 0.0001$.